Angewandte Chemie
Eine Zeitschrift der Gesellschaft Deutscher Chemiker

Supporting Information

Measurement of Angstrom to Nanometer Molecular Distances with ^{19}F Nuclear Spins by EPR/ENDOR Spectroscopy

Andreas Meyer, Sebastian Dechert, Surjendu Dey, Claudia Höbartner, and Marina Bennati**

anie_201908584_sm_miscellaneous_information.pdf

Content

1. Model Compounds

1.1. Synthesis

All reactants have been purchased from Acros Organics except for dicyclohexyl carbodiimide (Sigma Aldrich) and 4'-fluoro-4-hydroxybiphenyl (TCI) and were used as received.

3-(*o*-Fluorophenoxycarbonyl)-2,2,5,5-tetramethylpyrroline-*N*-oxyl **1**

221.3 mg (1.203 mmol) of 2,2,5,5-tetramethylpyrroline-*N*-oxyl-3-carboxylic acid, 135.6 mg (0.108 mL, 1.211 mmol) of *o*-fluorophenol, 295 mg (1.432 mmol) of *N,N*-dicyclohexylcarbodiimide and 16 mg *p*-(dimethylamino)-pyridine (0.131 mmol) were dissolved in 10 mL of THF. The yellow solution was stirred at room temperature and a colorless precipitate was observed after a few minutes. After stirring for 4 hours, the suspension was filtrated to remove the precipitate. After removing the solvent, the yellow raw product was subjected to column chromatography using a mixture of THF, DCM and hexane (1:3:9) as eluent and silica gel as stationary phase, yielding **1** as a yellow solid (220 mg, 66%). Crystals suitable for X-ray structure determination could be obtained by slow evaporation of a solution of **1** in a mixture of DCM and hexane.

ESI-MS: *m/z* 278.2 (40 %, $[C_{15}H_{17}NO_3F]^+$, $[M]^+$), 264.1 (100 %, $[C_{14}H_{15}NO_3F]^+$, $[M-CH_2]^+$). Elemental Analysis: Calcd.: C, 64.74; H, 6.16; N 5.05. Found: C, 64.55; H, 6.13; N, 5.05.

3-(*m*-Fluorophenoxycarbonyl)-2,2,5,5-tetramethylpyrroline-*N*-oxyl **2**

The synthesis, purification and crystallization of **2** proceed in analogy to the procedures used for **1** with a yield of 65%.

ESI-MS: *m/z* 278.2 (100 %, $[C_{15}H_{17}NO_3F]^+$, $[M]^+$), 264.1 (90 %, $[C_{14}H_{15}NO_3F]^+$, $[M-CH_2]^+$). Elemental Analysis: Calcd.: C, 64.74; H, 6.16; N 5.05. Found: C, 64.56; H, 6.22; N, 5.11.

3-(*p*-Fluorophenoxycarbonyl)-2,2,5,5-tetramethylpyrroline-*N*-oxyl **3**

The synthesis, purification and crystallization of **3** proceed in analogy to the procedures used for **1** with a yield of 68%.

ESI-MS: *m/z* 278.2 (90 %, $[C_{15}H_{17}NO_3F]^+$, $[M]^+$), 264.1 (100 %, $[C_{14}H_{15}NO_3F]^+$, $[M-CH_2]^+$). Elemental Analysis: Calcd.: C, 64.74; H, 6.16; N 5.05. Found: C, 64.69; H, 6.23; N, 5.07.

3-(*p*-(4-Fluorophenyl)phenoxycarbonyl)-2,2,5,5-tetramethylpyrroline-*N*-oxyl **4**

The synthesis and purification of **4** proceed in analogy to the procedures used for **1** with a yield of 69%. Crystals suitable for X-ray structure determination could be obtained by slow evaporation of a solution of **4** in mixture of acetone and hexane at 4 °C.

ESI-MS: *m/z* 356.2 (100 %, $[C_{21}H_{21}NO_3F]^+$, $[M]^+$), 340.1 (35 %, $[C_{20}H_{19}NO_3F]^+$, $[M-CH_2]^+$). Elemental Analysis: Calcd.: C, 71.17; H, 5.95; N 3.95. Found: C, 71.01; H, 5.97; N, 3.97.

HPLC chromatograms of all compounds are shown in Appendix B, Figure S22.

1.2. Crystallography

1.2.1. Experimental Details

Crystal data and details of the data collections are given in Tables S1 and S2. X-ray data were collected on a STOE IPDS II diffractometer (graphite monochromated Mo-Kα radiation, λ = 0.71073 Å) by use of ω scans at –140 °C. The structures were solved with SHELXT[1] and refined on F^2 using all reflections with SHELXL-2018.[2] Non-hydrogen atoms were refined anisotropically. Hydrogen atoms were placed in calculated positions and assigned to an isotropic displacement parameter of 1.2/1.5 U_{eq}(C). In **1**, one *o*-C_6H_4-F moiety was found to be disordered about two positions (occupancy factors: 0.847(2)/0.153(2)) in one of the two crystallographically independent molecules. In **2**, a fluorine and a hydrogen atom were disordered about the *meta*-positions of the phenyl-ring (occupancy factors: 0.909(3)/0.091(3)) in one of the two crystallographically independent molecules. In case of **4** the acetone solvent molecule was found to be disordered about a 2-fold rotation axis and was refined at ½ occupancy. RIGU restraints and EADP constraints were applied in case of **1**, DFIX restraints ($d_{C\text{-}H}$ = 0.95 Å) in case of **2**. Crystals of **3** were found to be twinned (twin law: –1 0 0, 0 –1 0, 0 0 1; BASF: 0.314(2)). A HKLF 5 format file was used for the refinement of the structure. Face-indexed absorption corrections were performed numerically with the program X-RED.[3]

Table S1. Crystal data and refinement details for **1** and **2**.

compound	**1 (am100)**	**2 (am101)**
empirical formula	$C_{15}H_{17}FNO_3$	$C_{15}H_{17}FNO_3$
formula weight	278.29	278.29
crystal size [mm³]	0.50 x 0.49 x 0.46	0.50 x 0.48 x 0.46
crystal system	monoclinic	monoclinic
space group	$P2_1/c$ (No. 14)	$P2_1/c$ (No. 14)
a [Å]	24.9335(6)	19.4468(5)
b [Å]	10.9218(2)	9.6159(2)
c [Å]	10.8646(3)	16.5589(4)
β [°]	101.092(2)	114.108(2)
V [Å³]	2903.36(12)	2826.40(12)
Z	8	8
ρ [g·cm^{-3}]	1.273	1.308
F(000)	1176	1176
μ [mm^{-1}]	0.097	0.100
T_{min} / T_{max}	0.7822 / 0.9586	0.8083 / 0.9818
θ-range [°]	1.665 - 26.798	2.295 - 26.912
hkl-range	±31, ±13, ±13	±24, ±12, ±20
measured refl.	39595	39153
unique refl. [R_{int}]	6150 [0.0269]	5998 [0.0331]
observed refl. ($I > 2\sigma(I)$)	5205	5177
data / restr. / param.	6150 / 108 / 382	5998 / 7 / 385
goodness-of-fit (F^2)	1.021	1.042
*R*1, *wR*2 ($I > 2\sigma(I)$)	0.0363 / 0.0897	0.0326 / 0.0824
*R*1, *wR*2 (all data)	0.0443 / 0.0958	0.0395 / 0.0859
res. el. dens. [e·Å^{-3}]	–0.280 / 0.366	–0.174 / 0.313

Table S2. Crystal data and refinement details for **3** and **4**.

compound	**3 (am102)**	**4 (am103b)**
empirical formula	$C_{15}H_{17}FNO_3$	$C_{21.75}H_{22.50}FNO_{3.25}$
formula weight	278.29	368.91
crystal size [mm³]	0.50 x 0.48 x 0.26	0.50 x 0.49 x 0.34
crystal system	monoclinic	monoclinic
space group	$P2_1/c$ (No. 14)	$C2/c$ (No. 15)
a [Å]	25.2416(11)	57.6975(17)
b [Å]	10.9243(3)	9.5380(2)
c [Å]	10.8144(5)	13.8658(4)
β [°]	101.154(3)	97.445(2)
V [Å³]	2925.7(2)	7566.3(4)
Z	8	16
ρ [g·cm^{-3}]	1.264	1.295
F(000)	1176	3120
μ [mm^{-1}]	0.096	0.093
T_{min} / T_{max}	0.9553 / 0.9799	0.3599 / 0.8225
θ-range [°]	1.645 - 26.240	1.424 - 26.920
hkl-range	±31, ±13, –11 to 13	±72, ±12, ±17
measured refl.	28864	50317
unique refl. [R_{int}]	28864	8026 [0.0511]
observed refl. ($I > 2\sigma(I)$)	17383	6357
data / restr. / param.	28864 / 0 / 370	8026 / 0 / 515
goodness-of-fit (F^2)	0.951	1.033
$R1$, $wR2$ ($I > 2\sigma(I)$)	0.0473 / 0.1229	0.0475 / 0.1363
$R1$, $wR2$ (all data)	0.0802 / 0.1585	0.0600 / 0.1453
res. el. dens. [e·Å^{-3}]	–0.263 / 0.251	–0.279 / 0.391

1.2.2. Depiction of the unit cells

Compound 1

Figure S1 shows the unit cell of **1** along the c-axis.

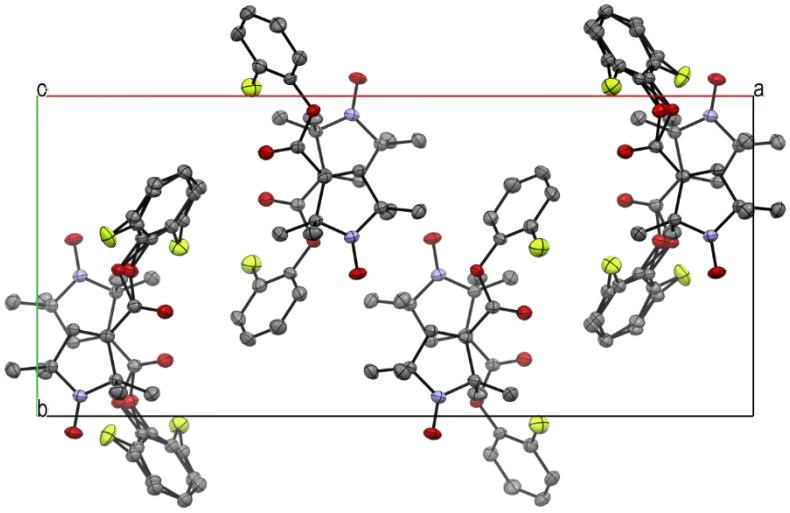

Figure S1. Unit cell of **1**. Color code: grey = carbon, red = oxygen, blue = nitrogen, yellow = fluorine. Hydrogen atoms have been omitted, ellipsoids at 50 % probability level. Depth cue is activated for clarity.

Compound 2

Figure S2 shows the unit cell of **2** along the b-axis.

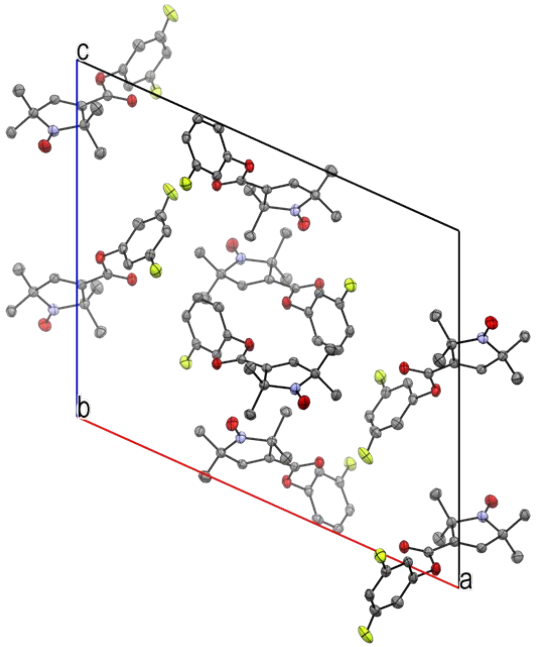

Figure S2. Unit cell of **2**. Color code: grey = carbon, red = oxygen, blue = nitrogen, yellow = fluorine. Hydrogen atoms have been omitted, ellipsoids at 50 % probability level. Depth cue is activated for clarity.

Compound 3

Figure S3 shows the unit cell of **3** along the c-axis.

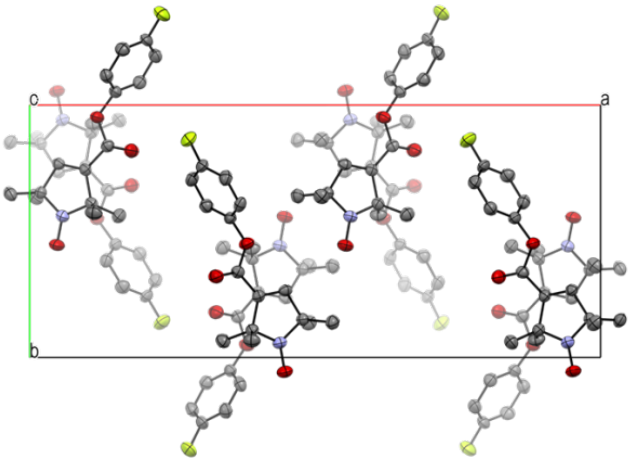

Figure S3. Unit cell of **3**. Color code: grey = carbon, red = oxygen, blue = nitrogen, yellow = fluorine. Hydrogen atoms have been omitted, ellipsoids at 50 % probability level. Depth cue is activated for clarity.

Compound 4

Figure S4 shows the unit cell of **4** along the *b*-axis.

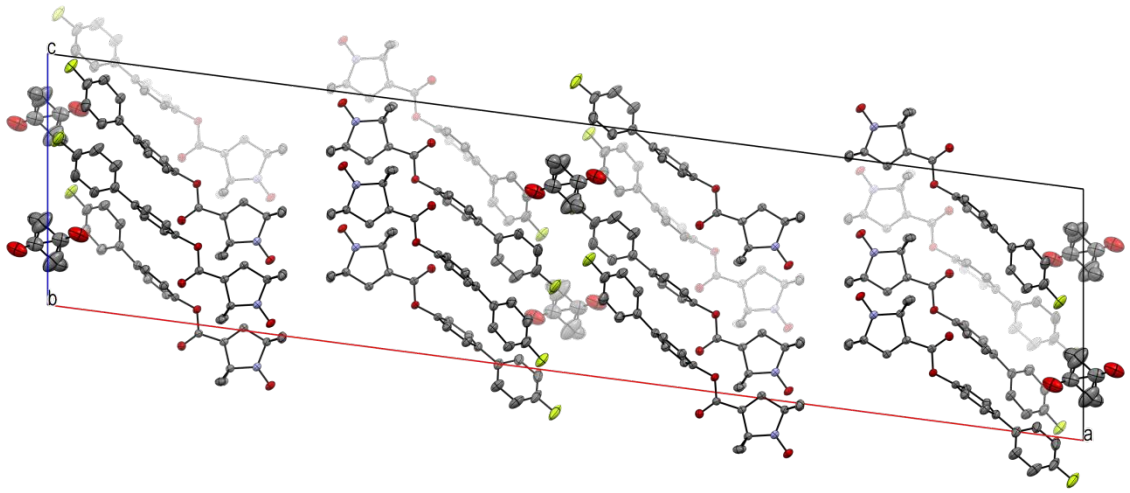

Figure S4. Unit cell of **4**. Color code: grey = carbon, red = oxygen, blue = nitrogen, yellow = fluorine. Hydrogen atoms have been omitted, ellipsoids at 50 % probability level. Depth cue is activated for clarity.

2. Synthesis and characterization of spin labelled RNA duplexes

2.1. Materials

Unmodified 2'-*O*-TOM-protected RNA phosphoramidite building blocks and 5'-*O*-DMT-2'-Fluoro deoxyadenosine (n-PAC) phosphoramidite were purchased from Carbosynth and ChemGenes. All other chemicals and HPLC grade solvents were purchased and used without further purification. Silica gel plates coated with fluorescent indicator were used for thin layer chromatography (TLC) and the plates were visualized with UV light. Silica gel 60, 0.032-0.063 mm (230-450 mesh) was used for column chromatography. Acrylamide/bisacrylamide stock solution was purchased, and polyacrylamide gels were prepared freshly before use by polymerization with ammoniumperoxodisulfate and tetramethyl ethylene diamine.

2.2. Methods

NMR spectra (^{1}H, ^{13}C and ^{31}P) were recorded using 400 MHz Bruker Avance III instrument. Chemical shifts are reported in parts per million (ppm) and were referenced to residual protium in the solvent. Coupling constants (*J*) are reported in Hz with the following multiplicity designations: s (singlet), d (doublet), t (triplet), q (quartet), doublet of doublet (dd), m (multiplet), and br (broad).

High-resolution ESI mass spectra in positive or negative ion mode were acquired on a Bruker micrOTOF-Q III.

2.3. Synthesis of convertible uridine phosphoramidite

5'-*O*-DMT-2'-*O*-TOM-O^4-(4-chlorophenyl)uridine 3'-cyanoethyl phosphoramidite (**S4**) was synthesized starting from uridine in four steps, following our previously reported procedure, which is summarized in Scheme S1.[4] For documentation of the quality of the batch used in this work, the ^{1}H and ^{31}P-NMR spectra of compound **S4** are given in Appendix C (Figures S23 and S24).

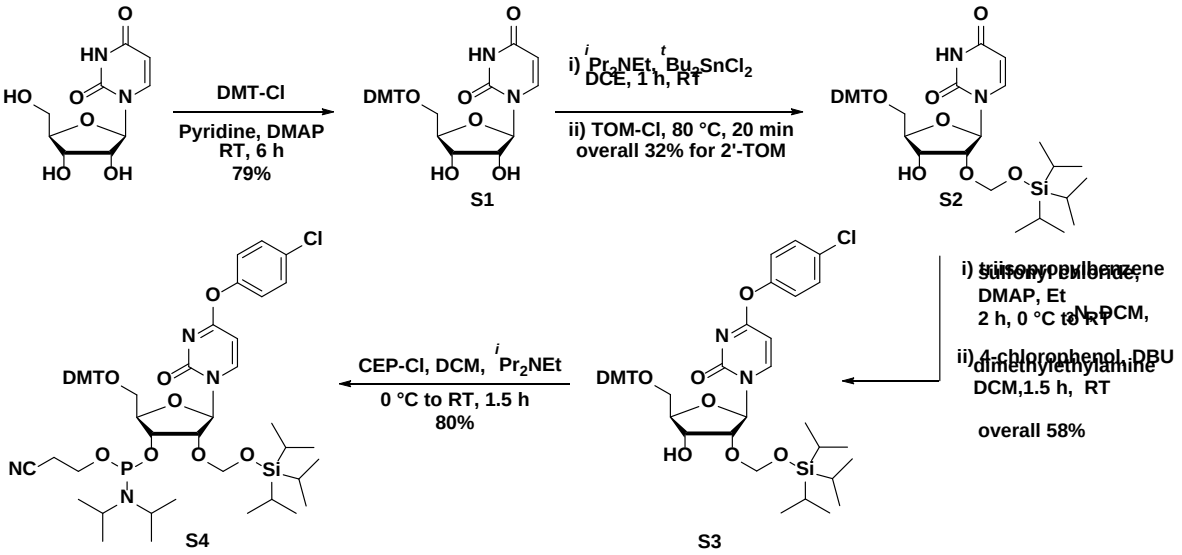

Scheme S1. Synthesis of 2'-*O*-TOM-protected convertible uridine nucleoside building block **S4.**

5'-*O*-(4,4'-Dimethoxytrityl)-2'-*O*-(triisopropylsilyl)oxymethyl-*O*^{4}-(4-chlorophenyl) uridine-3'-(2-cyanoethyl-N,N-diisoproyplphosphoramidite) (S4)

^{1}H NMR (400 MHz, $CDCl_3$): δ 8.46 (dd, *J* = 28.5, 7.4 Hz, 1H), 7.45 – 7.38 (m, 2H), 7.34 – 7.25 (m, 9H), 7.09 – 7.06 (m, 2H), 6.87 – 6.82 (m, 4H), 6.12 (t, *J* = 1.9 Hz, 1H), 5.58 (dd, *J* = 24.4, 7.4 Hz, 1H), 5.23 – 5.20 (m, 1H), 5.14 – 5.12 (m, 1H), 4.60 – 4.43 (m, 1H), 4.32 – 4.26 (m, 2H), 3.96 – 3.88 (m, 1H), 3.81 – 3.80 (m, 6H), 3.72 – 3.51 (m, 4H), 3.46 (td, *J* = 10.7, 2.4 Hz, 1H), 2.66 – 2.56 (m, 1H), 2.40 (t, *J* = 6.4 Hz, 1H), 1.17 – 1.08 (m, 10H), 1.06 – 1.03 (m, 20H), 0.99 (d, *J* = 6.8 Hz, 4H).

^{31}P NMR (162 MHz, $CDCl_3$): δ 149.91, 149.90.

HRMS (ESI^+): Exact mass calculated for $C_{55}H_{72}ClN_4NaO_{10}PSi$ $[M + Na]^+$, 1065.4336. Found 1065.4331.

2.4. Synthesis, purification and characterization of RNA oligonucleotides

The synthesis of RNA oligonucleotides (Table S3) was performed by solid-phase synthesis on a Pharmacia Gene assembler on 0.6 µmol scale, using 5'-*O*-DMT-2'-Fluoro-*N*^{6}-phenoxyacetyl-2'-deoxyadenosine 3'-cyanoethyl phosphoramidite for introduction of 2'-F-A in **RNA-A**. The TEMPO-modified RNAs (**RNA-B1** and **RNA-B2)** were prepared using phosphoramidite **S4**, followed by incubation of the CPG support with 2 M 4-Amino-TEMPO in methanol at 42°C for 24 hours, 2'-*O*-TOM deprotection with 1 M TBAF in THF at 25°C for 16 hours, and purification by polyacrylamide gel electrophoresis, as reported earlier.[4,5]

The quality of the purified RNAs was examined by denaturing anion exchange HPLC using a DNA-Pac PA200 column, 2x250 mm, at 80°C with 6 M urea (gradient 0-40% B, detection by UV absorbance at 260 nm, and by HR-ESI-MS (Table S4). HR-MS analyses were performed on a Bruker microTOF-Q III ESI mass spectrometer using 200 pmol of RNA sample. Optimized ESI source parameters were as follows: End Plate Offset -500 V, Capillary Voltage 3000 V, Nebulizer 0.4 Bar, Dry Gas 4.0 L/min, Dry Temperature 200 °C, Collision Energy 10.0 eV, negative ion mode. Recorded MS-spectra were deconvoluted using Maximum Entropy deconvolution.

HPLC chromatograms and mass spectra related to the RNA syntheses are shown in Appendix C in Figures S25 – S28.

RNA duplex samples for ENDOR spectroscopy were prepared by mixing two complementary RNA strands in equimolar ratio (**RNA1** = **RNA-A** + **RNA-B1**, **RNA2** = **RNA-A** + **RNA-B2**) followed by annealing in 10 mM sodium phosphate buffer, pH 7.0, in the presence of 100 mM NaCl (the sample was heated to 95°C for 2 min and then slowly cooled to 25°C within 30 min). The solvent was evaporated and the residue dissolved in D_2O to a final concentration of 250 µM RNA duplex and stored at -80°C.

Table S3. RNA oligonucleotides used in this work.

RNA	Sequence	Modification
RNA-A	5′-CAUCCGFUCUAGUGCC-3′	F = 2'-F-Adenosine
RNA-B1	5′-GGCAXUAGAUCGGAUG-3′	X = N^4-TEMPO Cytidin
RNA-B2	5′-GGCACUAGAUXGGAUG-3′	X = N^4-TEMPO Cytidin

Table S4. HR-MS results for RNA oligonucletides

RNA	Molecular formula [M]	Calculated[M]	Deconvoluted[M]	Δ (ppm)
RNA-A	$C_{150}H_{188}FN_{56}O_{110}P_{15}$	5016.6887	5016.7135	4.9
RNA-B1	$C_{163}H_{206}N_{66}O_{110}P_{15}$	5311.8619	5311.8935	5.9
RNA-B2	$C_{163}H_{206}N_{66}O_{110}P_{15}$	5311.8619	5311.8969	6.5

3. 94 GHz EPR spectroscopy: Experimental set up and data analysis

3.1. EPR sample preparation

EPR samples **1 – 4** were dissolved either at a concentration of ~300 µM (**1**, **2**, and **3**) or ~240 µM (**4**) in a mixture of deuterated DMSO and methanol (v/v = 40/60) immediately before the experiments. About 2 µL of these solutions were filled into quartz W-band EPR tubes (0.5 mm inner diameter, open at both ends) which were shock-frozen in liquid nitrogen prior to inserting them into the precooled cavity. The used solvent mixtures results in transparent, glassy samples upon rapid freezing. For the RNA samples, 250 µM solutions of RNA in deuterated sodium phosphate buffer (pH 7, 10 mM sodium phosphate along with 100 mM of NaCl, see section 2.4) were mixed with deuterated glycerol in a 2:1 volumetric ratio, giving a final RNA concentration of ~165 µM. 2 µL of these solutions were filled into quartz W-band EPR tubes (open at both ends) which were shock-frozen in liquid nitrogen yielding transparent, glassy samples.

3.2. EPR measurements

3.2.1. General settings

Pulsed EPR and ENDOR experiments at W-band (94 GHz) microwave (MW) frequency were performed on a Bruker Elexsys E680 EPR spectrometer equipped with a commercial Bruker ENDOR, cylindrical resonator (EN600-1021H) inserted into a helium gas flow cryostat. Using a 2 W MW amplifier, typical $\pi/2$ pulse lengths of 10 – 12 ns were achieved. Mims ENDOR experiments were performed at a temperature of 50 K, using RF pulses amplified with a 250 W RF amplifier (250A250A Amplifier Research). This yielded π pulse lengths as short as 22 – 25 µs for protons at the highest attainable RF power. Similar lengths could be used for ^{19}F nuclei at full power, as shown in Figure S5 by the Rabi oscillations recorded for the ^{19}F resonances on compound **1** at 0 and 8 dB RF1 attenuation. Inversion recovery and stimulated echo experiments were conducted with shot-repetition times (SRT) on the order of 4 – 30 ms, which were at least four times the spin-lattice relaxation time of the nitroxide under the used experimental conditions (see section 3.2.3). The ENDOR experiments were conducted using stochastic RF acquisition with 10 shots per point (SPP).[6,7] By comparison to experiments with 1 SPP it was found that saturation of ^{19}F spins was negligible under these conditions and a significant gain in sensitivity was achieved, as the change between points on the RF frequency axis requires about 30 ms and thus strongly reduces the averaging rate if only 1 SPP is used. The acquisition gate was set to a length of 20 – 24 ns and placed symmetrically around the maximum echo intensity (inset to Figure S5).

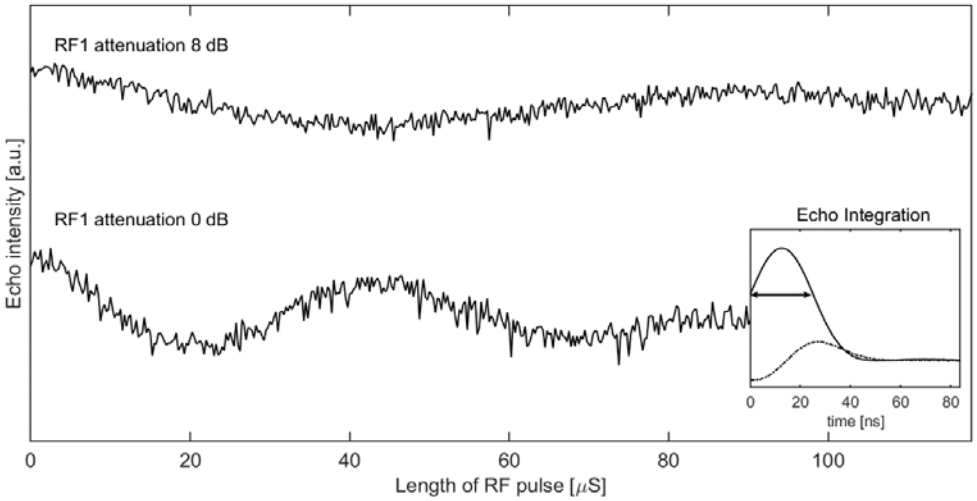

Figure S5. a) Rabi oscillations of ^{19}F nuclei at 0 and 8 dB. The inset illustrates the integration window used (full and dotted lines are the real and imaginary part of the stimulated echo).

3.2.2. Echo-detected EPR spectra

The echo-detected EPR spectra of all compounds were recorded with the two pulse echo sequence. The EPR spectra of compounds **1** – **4** were found to be virtually indistinguishable from each other. Likewise, the EPR spectra of both RNA samples were found to be indistinguishable, but they slightly differed from the spectra of the model compounds. Figure S6 shows the spectrum of **1** in frozen solution at 50 K as well as the EPR spectrum of **RNA1** along with EasySpin[8] simulations as examples. The spectra were simulated with EPR parameters typical for nitroxides[9] which are given in Table S5. The differences in the EPR parameters between compounds **1** – **4** and the RNA samples is attributed to the different polarities and H-bond donor abilities of the used solvent systems and is in line with previous observations on nitroxides (for more protic environments, g_x is expected to shift towards lower values while the hyperfine coupling constants increase slightly).[9] Interestingly, while the shape of the spectra is reproduced (in terms of resolved structures) in the simulations this is not the case for the relative intensities at the B || g_x, g_y and g_z orientation (i.e. the low field side, the maximum and high field side of the spectrum, respectively). This is mostly attributed to anisotropic relaxation (see below).

Table S5. EPR parameters used to simulate the echo detected EPR spectra of compounds **1** – **4** and the RNA samples.

Samples	g_x, g_y, g_z[a]	A_x, A_y, A_z (^{14}N) [MHz]	LWPP[b] [MHz]
1 – **4**	2.0093 (0.0003), 2.0064 (0.0001), 2.0025 (0.0000)	13, 13, 94	10, 2
RNA1 and **RNA2**	2.0090 (0.0003), 2.0064 (0.0001), 2.0025 (0.0000)	18, 16, 102	10, 5

[a] The values in parentheses give the values of *g* strain used in the simulation. [b] LWPP = peak-to-peak linewidth, the first value refers to the Gaussian contribution, the second to the Lorentzian contribution.

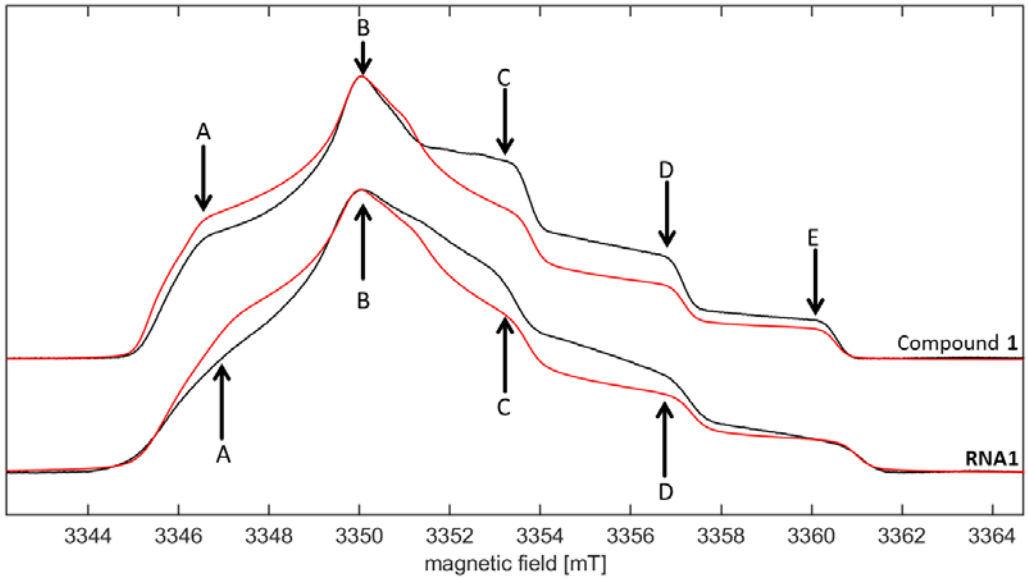

Figure S6. Echo-detected EPR spectra (black) at 50 K along with their simulation (red) of either **1** or **RNA1** (see labelling in the Figure). The simulation parameters are given in Table S5. The arrows mark the observer positions of the ENDOR spectra. SRT was 4 ms, SPP = 75, τ = 240 ns, 1 scan, acquisition time ~ 8 minutes for both spectra.

3.2.3. Relaxation measurements

a) Nitroxide Model Systems

The relaxation times have a large effect on the sensitivity of the ^{19}F-ENDOR distance measurements. Within a variation of ~±5%, the relaxation times were identical for all samples at the employed measurement conditions. The spin-lattice relaxation time of the electron T_{1e} determines the shot repetition rate and was measured using the inversion recovery experiment. Figure S7 shows the inversion recovery curve for **2** recorded at three different positions of the EPR spectrum. The recovery could be fitted by mono-exponential functions, indicating that the effect of spectral diffusion is weak. The obtained values were also in agreement with the echo intensities observed on the SpecJet upon variation of the shot-repetition time. Nevertheless, the values are only an estimate, as the inversion recovery curve might be affected by spectral diffusion.

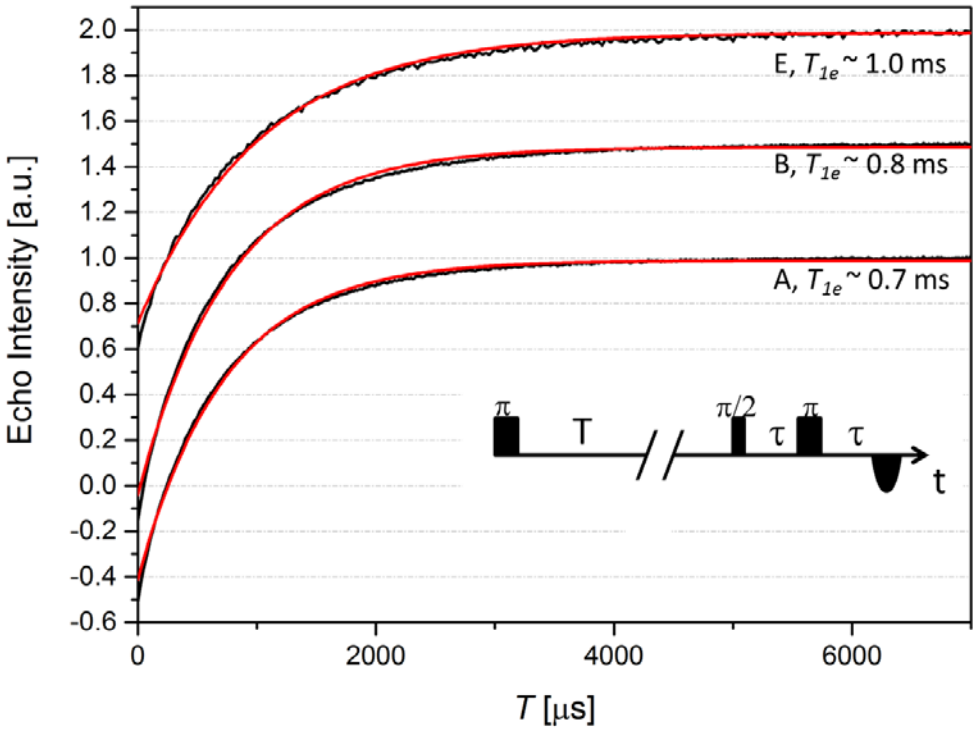

Figure S7. Inversion-recovery time traces of **2** (black) at 50 K along with mono-exponential fits (red). The pulse sequence is shown as inset, the interval *T* is varied. SRT = 10 ms, SPP = 5, τ = 240 ns, initial *T* value of 1 µs, 1 scan. For better visibility, traces B and E are shifted by 0.5 or 1 intensity unit, respectively.

The phase memory time T_M is empirically defined as the loss of phase coherence during the intervals, in which the magnetization is located in the xy-plane (i.e. the τ intervals)[10] and is critical for measuring long distances. T_M is often measured using the two-pulse (π/2-τ-π-τ) echo experiment. However, T_M in Mims ENDOR depends strongly also on the time interval *T* (see Figure S8 for the assignment of the intervals). Therefore, T_M was measured by monitoring the intensity of the stimulated echo when varying τ for different, fixed values of *T*. The echo intensity *I* in dependence on the τ value for a given *T* was fitted using eq. (S1):

$$I = I_0 e^{-2\tau/T_M} \qquad \text{(S1)}$$

For the model systems **1** – **4**, eq. (S1) yielded extremely good fits of the experimental data, whereas the data of the RNA molecules are only approximated by a monoexponential function. Notice that ambiguity in the value of T_M arises depending on whether or not the factor "2" is included in the argument of the exponential. In this work, the factor is included to acknowledge the loss of phase coherence in both τ intervals. The obtained T_M values as a function of τ for fixed *T* values at three different observed positions in the EPR line are shown in Figure S8. The T_M values for *T* = 1 µs are similar to those obtained by the two-pulse echo experiment, but they decrease significantly when increasing *T* to values relevant for resolving small couplings in ^{19}F Mims ENDOR, i.e. ≳ 50 µs. Furthermore, a slight anisotropy is found for T_M (under the conditions used for Mims ENDOR, T_M varies by about 500 ns for the three displayed observer positions). The values obtained at the y positions were those which were used for choosing τ in the Mims ENDOR experiments. This relaxation anisotropy contributes to the discrepancy between the intensities of the simulated EPR spectrum and the experimental spectrum.

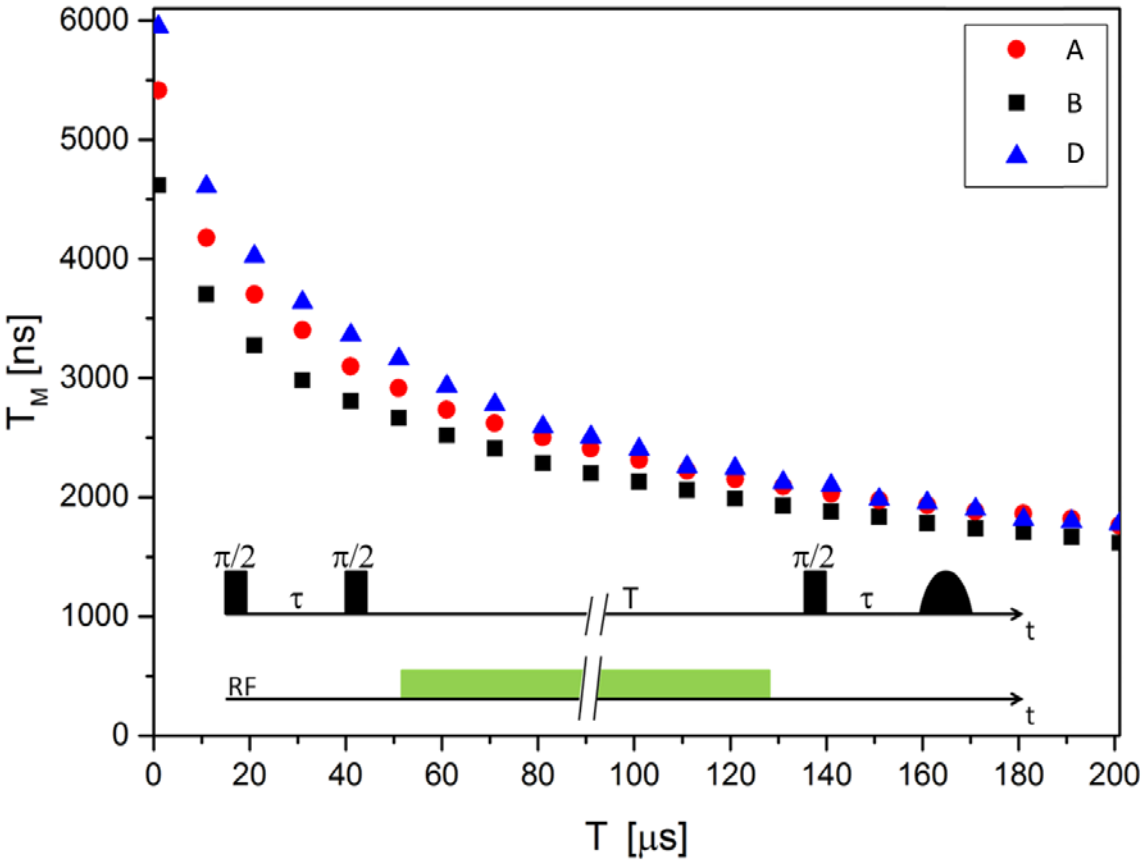

Figure S8. Phase memory times T_M of **1** according to eq. (S1) recorded by incrementing τ and for different values of T at three different observer positions. The inset shows the Mims ENDOR sequence. When measuring the relaxation times, the RF pulse is omitted and the value of τ is varied for a fixed value of T. Values were extracted from the echo decay curve by using a mono exponential fitting function.

b) RNA Molecules

The relaxation time constants in the RNA molecules were found to be similar to those obtained in the model systems. As a consequence, similar experimental parameters as used for the nitroxide model systems could be used in the ENDOR measurements on the RNA systems.

The inversion recovery curves obtained for the nitroxides in **RNA1** and **RNA2** are shown in Figure S9.

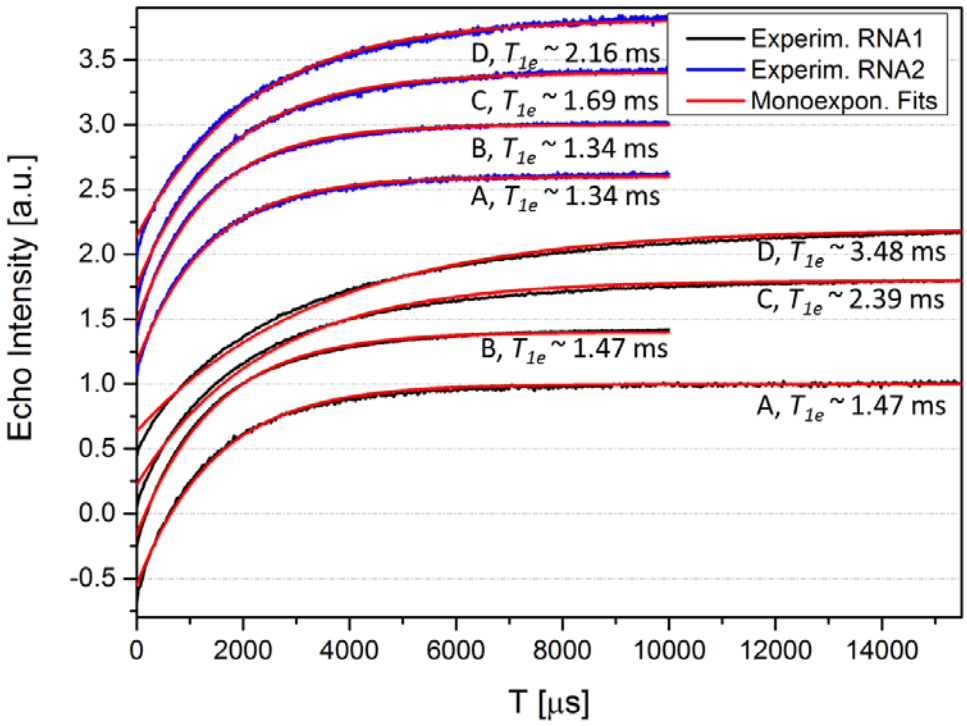

Figure S9. Inversion-recovery time traces of **RNA1** (black) and **RNA2** (blue) at 50 K along with mono-exponential fits (red). The pulse sequence is shown in Figure S7, the interval *T* is varied. SRT 10 – 30 ms, SPP = 5, τ = 240 ns, initial *T* value of 1 µs, 1 scan. For better visibility, the traces (except A for **RNA1**) are shifted along the intensity axis.

The phase memory times obtained by fitting a mono-exponential decay function to the echo decay curve as function of τ are shown in Figure S10. Noteworthy, the phase memory times of the nitroxides in both RNA samples are slightly shorter than those for the model compounds under the conditions used for Mims ENDOR (i.e. *T* ~ 54 µs) and less anisotropic. Figure S10 also contains an exemplary echo decay curve as inset recorded using a *T* interval similar to what was used in ENDOR experiments.

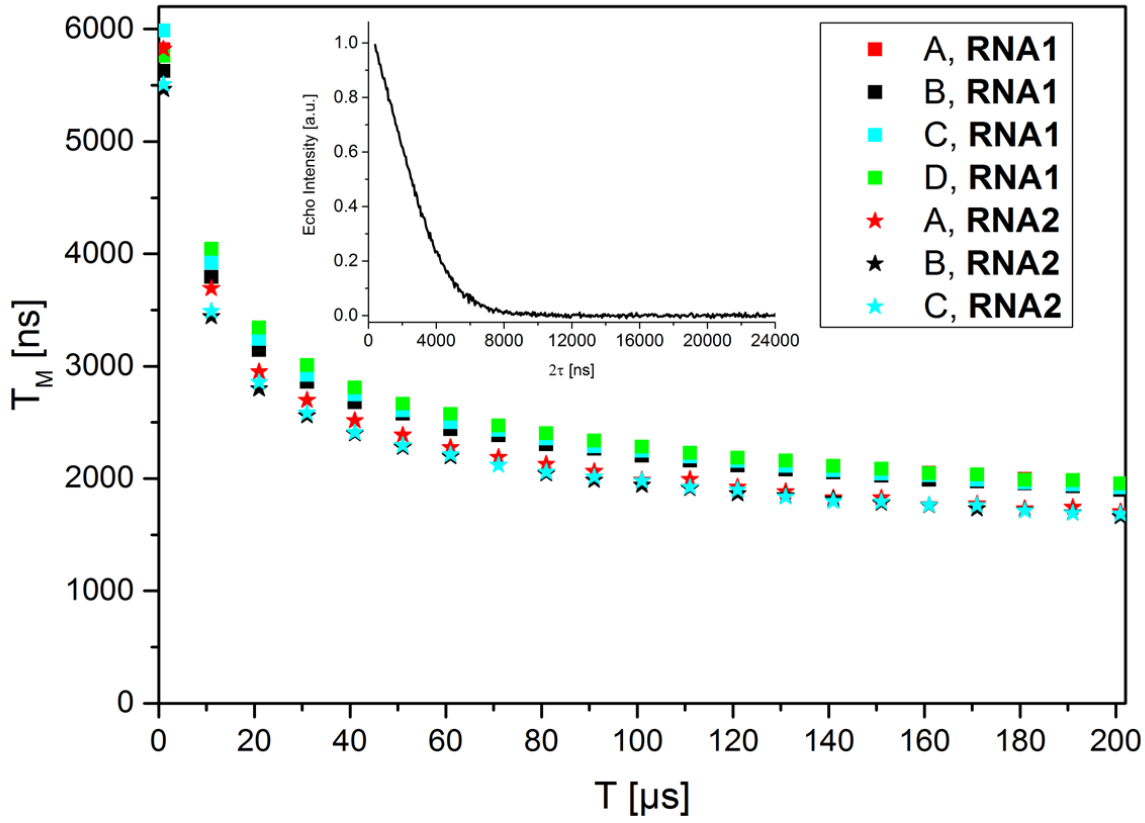

Figure S10. Phase memory times T_M of **RNA1** (squares) and **RNA2** (stars) according to eq. (S1) recorded by incrementing τ and for different values of T at three different observer positions. The pulse sequence is shown in Figure S8. When measuring the relaxation times, the RF pulse is omitted and the value of τ is varied for a fixed value of T. Values were extracted from the echo decay curve by using a mono-exponential fitting function as an approximation. The inset shows an exemplary echo decay curve taken with a T value of 50 µs.

3.2.4. Optimizing the ENDOR sensitivity

The sensitivity S of the experiment at a given temperature can be expressed by the product of the echo intensity I and the ENDOR efficiency F (eq. (S2)):

$$S = F \cdot I \tag{S2}$$

The echo intensity I decays as a function of τ as already given in eq. (S1) whereas the ENDOR efficiency F is a periodic function depending on the hyperfine coupling constant A and the value of τ (eq (S3)):[11]

$$F = 0.5 \cdot sin^2(2\pi \frac{A}{2} \tau) \tag{S3}$$

Since I decreases monotonically with τ while F increases monotonically up to the first maximum with increasing τ, a compromise between I and F has to be sought. One possibility is to plot S and find the maximal value depending on τ, as shown in Figure S11 for the nitroxide model systems **1** – **4** for an RF pulse of ~54 µs (the interval T is equal to the RF pulse length plus 1 µs before and after the pulse). The Figure shows that the maximal sensitivity S_{max} drops considerably for larger distances R and the

optimum value τ_{opt} increases markedly. Figure S11 also shows that the optimal τ value for the parallel and the perpendicular orientation, but also for all other orientations, is different. To avoid complications in data analysis when summing up the orientation selective spectra, a constant value of τ was chosen for the experiments at all observer positions, optimized for the expected value of the parallel component of the hyperfine tensor (i.e. $2T$) and the T_M value at the maximum of the EPR spectrum. This choice yields sufficient values of S in every region of the Pake pattern. In all ENDOR measurements, optimized τ values have been used.

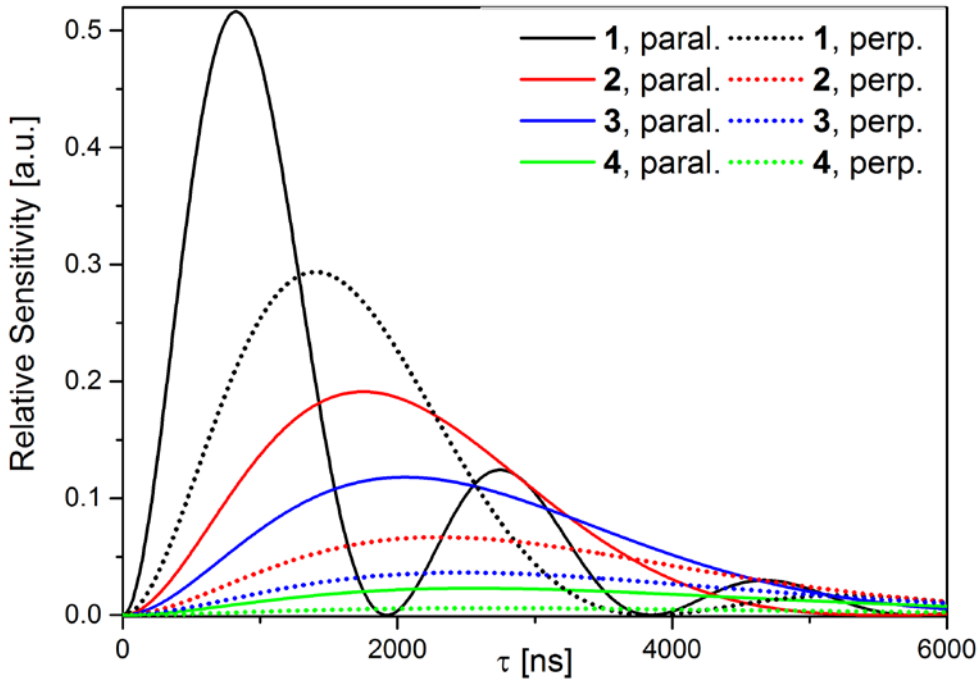

Figure S11. Calculated, relative sensitivities S for the parallel and perpendicular components of the hyperfine coupling tensors of **1** – **4**. For the calculations, dipolar coupling constants T of 260, 90, 64 and 25 kHz have been chosen for **1** – **4**, respectively, along with a phase memory time T_M of 2700 ns. The τ_{opt} values for the parallel component (equal to $2T$) are then located at approximately 820, 1750, 2030 and 2550 ns for **1** – **4**, respectively.

3.3 Orientation selective spectra of 2 and 3

The orientation selective Mims ENDOR spectra of **2** and **3** are depicted in Figure S12. In analogy to **1** and **4**, resonances separated by T (corresponding to a prevalence of a perpendicular orientation of the inter-spin vector with respect to the external magnetic field) are observed at observer positions B – E, whereas couplings approximately twice as large (inter-spin vector parallel to the external field) is obtained at position A. The simulations of the spectra are also shown. Remarkably, despite using an ENDOR linewidth parameters differing by only 1 kHz in the simulations of **2** and **3**, the full widths at half maximum of the peaks in the orientation selective spectra are 4 – 5 kHz (positions B – D) or even ~15 kHz (position A) broader in the case of **2**, which is in large attributed to the presence of two unresolved, major conformers contributing to the spectra in the case of **2**, whereas only one major conformer is present in **3**. The simulation parameters are tabulated in the main text and explained in detail below.

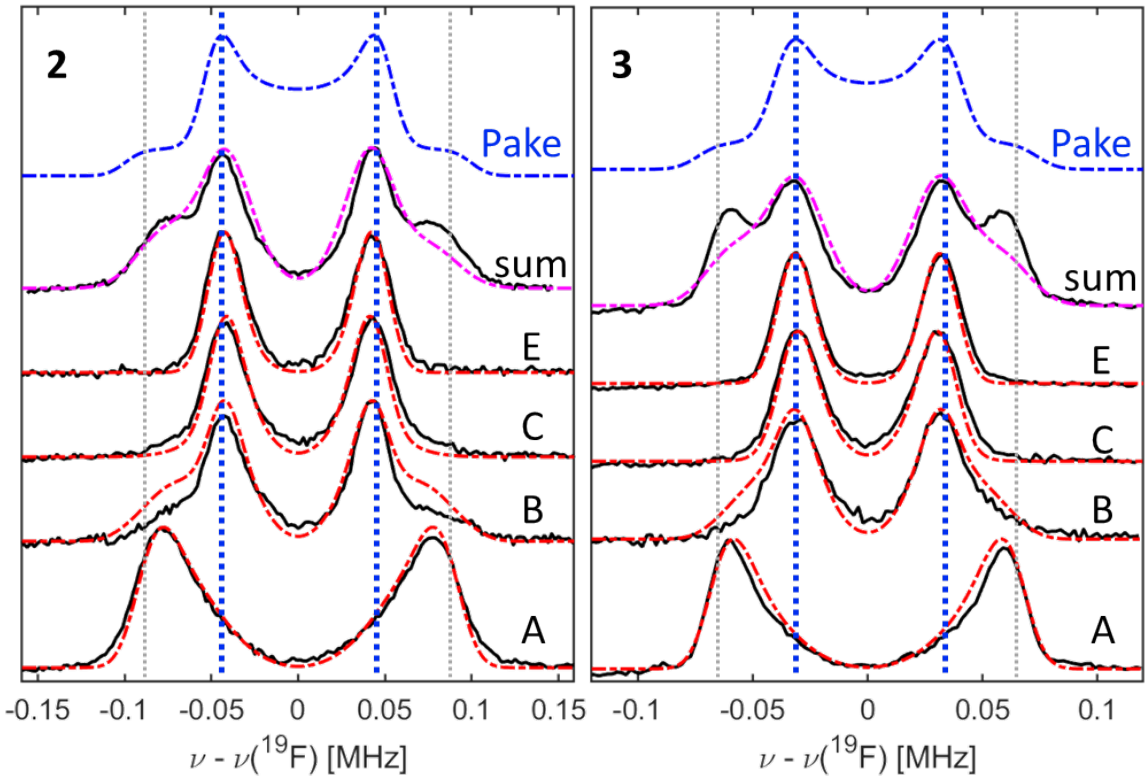

Figure S12. 94 GHz-^{19}F Mims ENDOR spectra of samples **2** and **3** (black lines) recorded at EPR resonance A to E, as marked on the right side. Top spectrum is the sum of the orientation selective spectra. Mims ENDOR simulations with (red) and without (purple) orientation selection are superimposed. The blue dashed spectrum represents the corresponding undistorted Pake pattern using same linewidth as for the simulation. Sum spectra contain 10401 and 18914 scans, respectively. Optimized τ values were 1730 (**2**) and 2000 ns (**3**), respectively. These values were kept fixed at each field excitation position. Further parameters: MW pulses 10 - 12 ns, shots-per-point (SPP) = 10, shot-repetition-time (SRT) = 4 ms, RF-pulse lengths 54 μs.

3.4 Effect of the RF power

The measurements on **1** – **3** presented in the main text and above have been performed using attenuated RF pulses with lengths on the order of 50 µs (**1** – **3**) to increase the spectral resolution. The effect is illustrated in Figure S13, which shows the data and simulations for **2** and compares them to data obtained using RF pulse lengths of only 25 µs with RF power adjusted accordingly. As can be seen, the ENDOR linewidth is markedly higher when using the shorter RF pulses and resolution is lost. This is especially notable in the singularities corresponding to the perpendicular components of the HFC tensor in the orientation selective spectra, which are considerably broadened, and also no longer fully resolved in the sum spectrum.

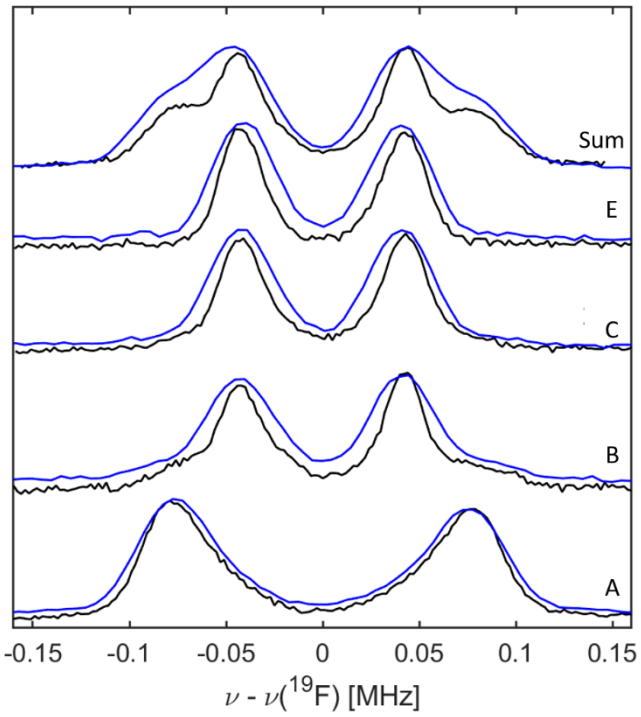

Figure S13. Spectra of **2** using RF pulse lengths of 50 µs (black lines) and spectra obtained using pulse lengths of 25 µs along with their simulations (blue lines). The ENDOR linewidth in the blue spectra is increased by ~15 kHz.

In the case of **4**, it was found that the length of the RF pulse needs to be even further increased to 110 µs in order to improve the spectral resolution (see Fig. 1 main text). Figure S14 shows spectra of **4** recorded with RF pulse lengths of 54 µs. Notably, the doublet structure at position **B** – **D** is hardly visible, and the two features of the Pake pattern are neither resolved in the sum spectrum nor in the simulation without orientation selection. The peak positions in the summed spectra appear at 28 – 29 kHz separation, which lies in between the parallel and the perpendicular component of the coupling tensor of **4**.

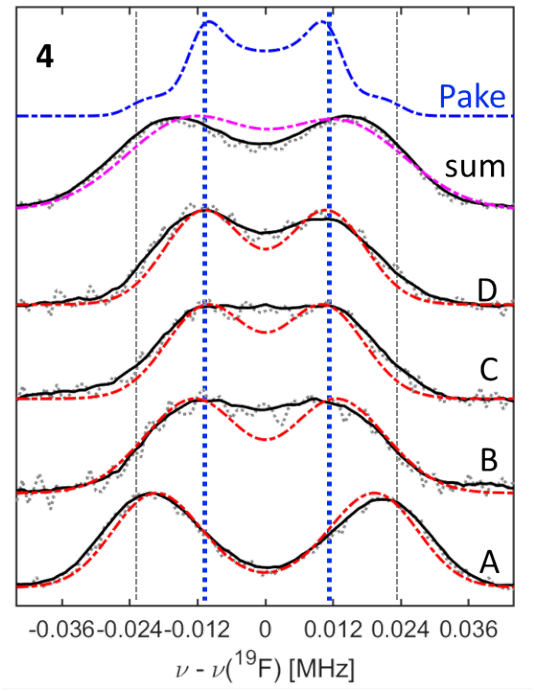

Figure S14. Spectra and corresponding simulations of **4** using RF pulse lengths of 54 µs and a τ value of 2550 ns (black, full and dashed lines respectively) The ENDOR linewidth used in the simulations is 16 kHz, all other parameters as in Table **1** in the main text.

3.5 Resolution of distances

The spectral data for compounds **1** – **4** as well as for the RNA systems was interpreted taking into account several isomers or broadening owed to a distribution of conformations. However, it was not possible to clearly resolve individual isomers in any system. The resolution is affected by several effects like the orientation selection, power broadening, specifics of the distance distribution (i.e. how many conformations are present and what are their populations, etc...). In the study presented herein, power broadening is identified as a major source of broadening, which limits the resolution. We suspect that clear resolution of spectral features requires separation of these features in excess of the ENDOR linewidth. To that end, the spectra of **2** and **3** merit consideration. The T_{read} values of these compounds differ by ~ 23 kHz, which is slightly above the ENDOR linewidth used in the simulations for **2** and **3**. To investigate whether or not we would be able to resolve the two compounds in a mixed sample, we summed up their respective spectra normalized to identical height at position A and B as well as their sum spectrum (**2** in red, **3** in green, the sum in black, Figure S15). This approach is justified, as the spectra in a hypothetical, mixed sample of **2** and **3** should be additive and we used similar measurement parameters for both compounds. Furthermore, it allows us to scale the two contributions to the addition spectra to equal height, so that we can focus the discussion here only on the linewidths and separation of certain spectral features, without having the additional complications of possibly different heights of the two contributions to the spectrum. In each spectrum shown in Figure S15, the positions at $\pm T/2$ and $\pm T$ are indicated by dotted and dashed lines, respectively. In spectrum A, the parallel component is selected, which should facilitate the separation of spectral features. Indeed, the maxima of the spectra of **2** and **3** at position A are separated by ~24 kHz, which is in agreement with expectations based on T_{read} values. As their separation exceeds the ENDOR linewidth, these features should be resolved, which is indeed observed in the black addition spectrum. The spectra at position B are dominated by the perpendicular contributions. Correspondingly, the maxima of the two compounds are separated by approximately half the distance as compared to position A, i.e. ~13 kHz. This value is below ENDOR linewidth. Consequently, these peaks would not be resolved, as the addition spectrum (black) confirms. Instead, a single peak which has its maximum at approximately the average frequency of the two contributions is obtained. Furthermore, the resulting peak is broader than the peaks of the individual species. As already mentioned in section 3.3, the two conformers **2a** and **2b** in the simulations of compound **2** behave completely analogous. Finally, the black sum spectrum reveals three resolved features. While direct assignment of the features to a certain coupling constant would no longer be possible, the presence of three features requires the presence of at least two different interspin distances, as a maximum of two features is expected in case of purely dipolar coupling. Notably, all resolved features in the black sum spectrum are separated by more than the ENDOR linewidth.

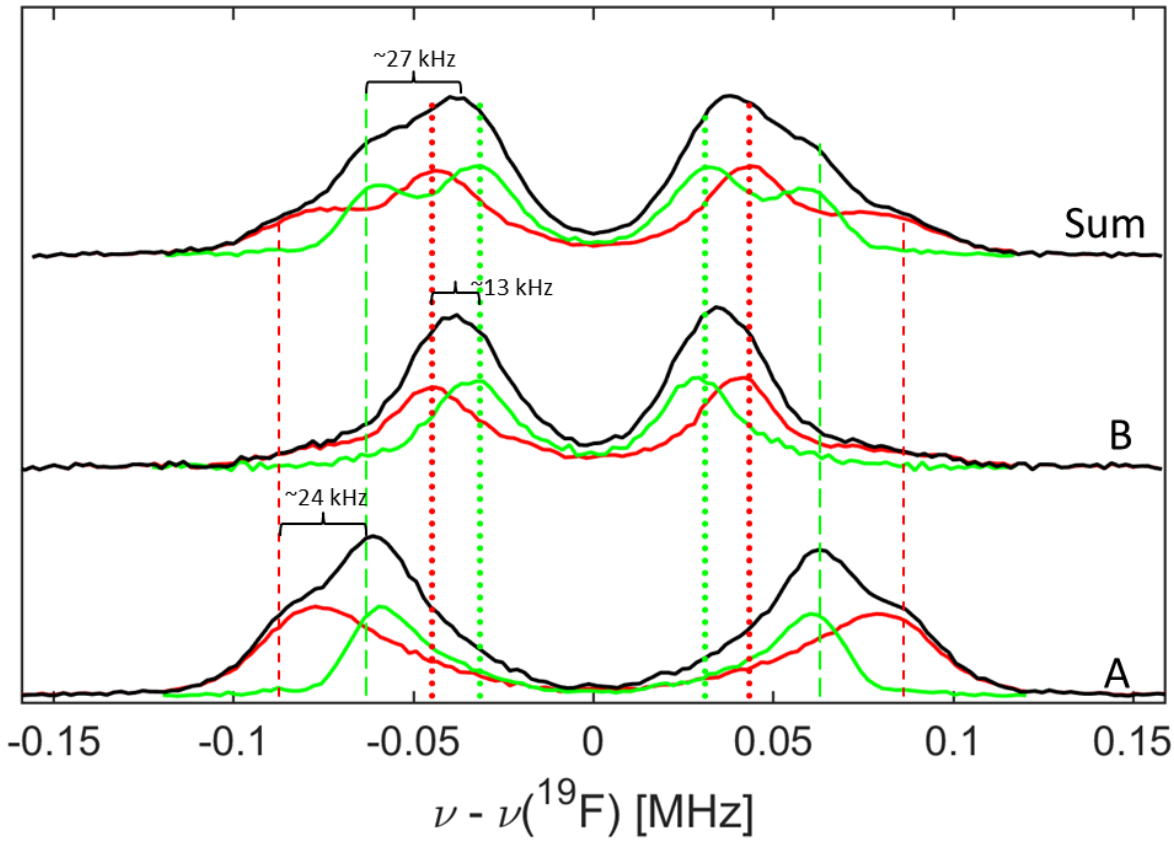

Figure S15. Spectra of **2** (red) and **3** (green), normalized to same height, as well as their addition in black. The observer position is indicated, the dotted lines are placed at ±T/2, the dashed ones at ±T. Spectral features separated by more than the ENDOR linewidth of ~19 kHz are resolved in the addition spectra (black).

4. Combined DFT/ENDOR analysis for model systems

4.1. Simulating orientation selective spectra

Orientation selected spectra contain information on the relative orientation of the *g* tensor to the hyperfine tensor. In the framework of a purely dipolar interaction the largest coupling frequency $2T$ is expected when the external magnetic field is parallel to the inter-spin vector, according to Eq. S4:

$$\upsilon_{HFC} = T(3\cos^2\theta - 1) \qquad \text{(S4)}$$

To describe the orientation of the inter-spin vector with respect to the N–O bond (i. e. the *x*-direction of the *g* tensor frame), two Euler angles α and β are introduced, see Fig.1g in the main text. These two angles describe a rotation of the *g* tensor frame into the dipolar tensor frame, i.e. a first rotation around the g_z axis (perpendicular to the plane of the pyrrolin ring) by α and then a second rotation by β around the *y'* axis (i.e. the *y* axis in the new coordinate system). Note that we define the parallel component of the coupling tensor as its *x* component (i.e. $T_x = 2T, T_x = T_y = -T$, see also below). Computation of orientation selected ENDOR spectra was performed using the software *EasySpin,* the EPR parameters reported in Table S6 and the Euler angles as obtained from the DFT optimized structures (Fig. 1g in the main text).

4.2. Geometry optimizations and calculations of EPR parameters

Starting point of the DFT calculations was always a geometry optimization using the unrestricted Kohn-Sham formalism with the TPSSh functional[12] and the svp basis set[13] as implemented in ORCA.[14] The starting structure for the optimization at the SVP level was obtained using the chemical graphics program Avogadro.[15] After the initial optimization, the structure was reoptimized at a higher level using the same functional but with the def-tzvp basis set[16] and the D3BJ dispersion correction.[17–19] Then, relaxed surface scans were performed in which the fluorophenyl group (compounds **1** and **2**) was rotated in 10° steps, again at the lower svp level. This led to up to two stable conformers with markedly different nitroxide-fluorine separations, which were reoptimized at the def2-tzvp level. Subsequently, a relaxed surface scan in which the pyrrolin ring was rotated was conducted for all compounds. In total, this led to up to four stable conformers, as mentioned in the main text, from which the Euler angles for the dipolar coupling tensor were extracted using a home-written program. For each optimized geometry, the hyperfine coupling parameters were also calculated with ORCA at the same level as the final geometry optimizations.

Even though similar torsional angles as those displayed by the in the crystal structures of **1** – **4** have been observed previously in related molecules,[20–22] the perpendicular orientation of the phenyl ring appears unusual and is probably caused by crystal packing. To investigate the torsional angles, relaxed surface scans, in which ϕ (dihedral angle between phenyl and carboxylate mean plane) and η (dihedral angle between pyrroline and carboxylate mean plane) were varied, have been conducted using DFT as implemented in ORCA, leading to the conformers shown in Figure 3 in the main text. The geometrical parameters of each structure obtained from DFT or from the crystal structures are listed in Table S6. Note, that conformers **a** and **b** as well as **c** and **d** are equivalent for compounds **3** and **4**. Furthermore,

conformer **d** was not found for **1**. Remarkably, conformers **a** yield geometrical parameters *R*, α and β that are very similar to the crystallographic values for all compounds.

Table S6. Selected geometrical parameters for **1** – **4**. The error in the DFT calculated structural parameters is likely less than about 10%.

	ϕ [°]	η [°]	R^b [Å]	α [°]	β [°]	$T_{calc}{}^c$ [kHz]
1, XRD[a]	75	4	6.8	-164	-19	241
1a, DFT	68	5	6.7	-162	-19	245
1b, DFT	43	5	7.2	-178	-13	202
1c, DFT	70	6	6.5	-149	19	269
2, XRD[a]	83	2	9.4	-162	16	90
2a, DFT	43	3	9.4	-156	-11	91
2b, DFT	53	2	9.7	-173	-11	81
2c, DFT	40	1	9.3	-151	11	92
2d, DFT	44	3	9.0	-129	7	104
3, XRD[a]	89	11	10.6	-164	4	63
3a, DFT	49	1	10.6	-164	0	64
3c, DFT	48	3	10.2	-140	-2	71
4, XRD[a,d]	70/35	13	14.8	-169	8	23
4a, DFT[d]	46/14	4	14.8	-164	-5	23
4c, DFT[d]	40/3	10	14.5	-139	5	25

[a] XRD = X-ray diffraction. For all compounds, two independent molecules were observed in the asymmetric unit with essentially identical geometries. The data in the table correspond to the molecules shown in Figure 1 in the main text. [b] Distance taken from the midpoint of the N-O bond as indicated in Figure 1 in the main text. [c] Values calculated using Eq. (1) from the main text. [d] **4** has a biphenyl substituent, the two values correspond to the angle between the planes of the carboxylate and the phenylene or the *p*-fluorophenyl groups, respectively.

4.3. Approach for ENDOR simulations using DFT derived parameters

Our approach to simulate the ENDOR spectra consisted in using a single coupling constant T given by eq. (1) in the main text to describe the elements of the dipolar coupling tensor $\boldsymbol{T}_{dip}$ (Eq. (S5)):

$$\boldsymbol{T}_{dip} = \begin{bmatrix} 2T & & \\ & -T & \\ & & -T \end{bmatrix} \qquad \text{(S5)}$$

On the other hand, the software ORCA does not use such simplifications and provides three dipolar tensor components plus one isotropic coupling constant (Eq. (S6)):

$$\boldsymbol{T}_{ORCA} = \begin{bmatrix} T_1 & & \\ & -T_2 & \\ & & -T_3 \end{bmatrix} + a_{iso} \qquad \text{(S6)}$$

In all cases encountered in this study, the dipolar tensor calculated by DFT was still close to the axially symmetric tensor (i.e. $0.5 \cdot T_1 \approx T_2 \approx T_3$ and $a_{iso} \approx 0$). Therefore, we introduce the approximation:

$$T_{DFT} \approx 0.5 \cdot T_1 \qquad \text{(S7)}$$

A comparison between simulations using the parameters listed in Table 1 and the simulations using the full tensor T_{orca} (Table S7 and eq. (S6)) is presented in Figures S16 and S17 and demonstrates that the approximation is suitable.

Table S7. Hyperfine coupling constants for all conformers of **1** – **4** calculated by DFT as defined by Eq. (S6). The error in the computed parameters is estimated to be less than 10%.

	T_1[kHz]	T_2[kHz]	T_3 [kHz]	a_{iso}[kHz]
1a	511	268	243	-5
1b	419	218	200	-1
1c	566	285	279	2
2a	190	99	91	-3
2b	166	86	80	-6
2c	201	113	88	-8
2d	218	120	99	-7
3a	122	71	51	3
3c	134	83	51	6
4a	47	24	21	1
4c	46	28	18	2

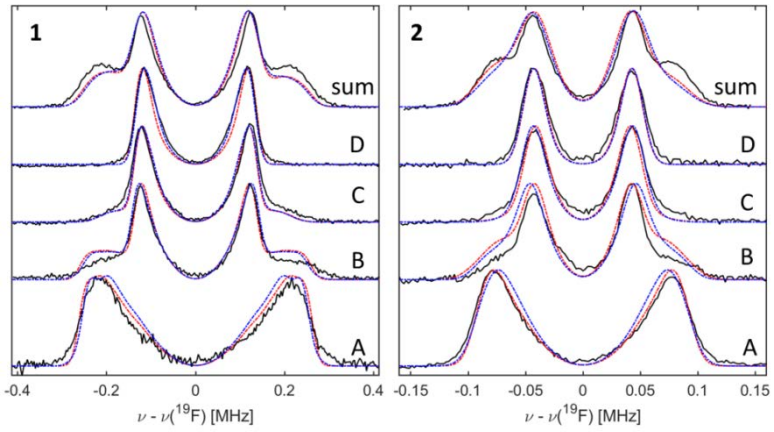

Figure S16. Spectra of **1** and **2** (black, full lines) along with simulations including all conformers using T_{sim} as given in Table 1 in the main text (red dashed lines) and using the coupling constants calculated by DFT given in Table S7 (blue, dashed lines).

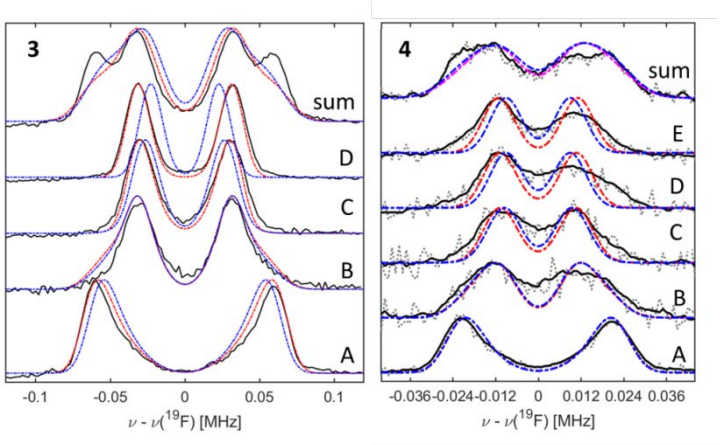

Figure S17. Spectra of **3** and **4** (black, full lines) along with simulations including all conformers using T_{sim} as given in Table 1 in the main text (red dashed lines) and using the coupling constants calculated by DFT given in Table S7 (blue, dashed lines).

Figures S16 and S17 show that in all cases except for **3** the DFT derived hyperfine tensor values T_{DFT} (Table S7) yield simulations of similar quality to those obtained by the approximation of Eq. (S7). Noteworthy, even in the apparently worst case of **3** the deviation between simulated and experimental spectra amounts to only a few kHz and appears within the precision of the DFT calculation.

5. Molecular Models of RNA1 and RNA2

It was previously established that C^T labelled RNA molecules retain the A-form.[23] Thus, the C^T spin label was introduced in a 16-mer duplex RNA molecular model in its A-form by superimposing the cytosine part of the C^T label with the respective cytosine base at the labelling position in the unlabeled RNA strand. To find the correct conformation of the C^T label in the RNA, previous data which reported six minimum conformations **a** – **f** were used as displayed in Figure S18.[23] Conformers **d** – **f** were discarded, since only conformers **a** – **c** allow effective base pairing, which is a requirement to retain the A-form of the RNA strands. Conformers **a** and **b** are almost isoenergetic and located in a wide basin of low energy conformations. Conformer **c** is already notably higher in energy, but also represents a (local) energy minimum in a region where less conformational freedom is inferred from the potential energy surface. To sample the potential energy surface more thoroughly, further conformers **g** – **o** were generated. Conformer **g** is placed near the centrum of the broad basin of low energy conformers in the potential energy surface whereas **h** – **n** are placed more towards the edges of the basin. Conformer **o** is a second conformation in the local energy minimum centered around conformer **c**. The geometrical parameters and resulting coupling constants of each conformer specified above for **RNA1** and **RNA2** are listed in Table S8. In addition, close interatomic contacts between non-hydrogen atoms of the C^T label and the surrounding RNA backbone have been counted, excluding the base which forms a hydrogen bonded pair with C^T. High numbers of such contacts indicate that the label clashes with the backbone.

Table S8. Geometrical parameters of the C^T conformations in **RNA1** and **RNA2**.

	R [Å]	T^a [kHz]	α [°]	β [°]	ϕ_1/ϕ_2 [°]	Within uncertainty of T_{read}/T_{sim}	Contacts below 2.9 Å
RNA1							
a	14.8	23	-72	-46	162/-13	No/No	10
b	12.2	41	-38	3	77/13	Yes/No	0
c	13.2	32	58	-7	-60/1	No/No	7
g	13.4	31	-58	-17	120/0	No/No	3
h	15.3	21	-87	11	120/-40	No/No	14
i	17.0	15	-114	-57	-165/-40	No/No	28
j	13.4	31	-31	-52	162/13	No/No	6
k	12.3	40	-8	-37	120/41	Yes/No	0
l	13.2	33	-53	30	77/-13	No/No	2
m	12.6	38	2	-43	77/61	Yes/No	5
n	11.8	45	-23	11	47/20	Yes/Yes	0
o	11.5	49	11	1	-60/41	Yes/Yes	1
RNA2							
a	12.8	35	155	33	162/-13	No/No	11
b	14.2	26	159	1	77/13	Yes/Yes	1
c	14.0	27	-6	-60	-60/1	Yes/Yes	12
g	13.6	29	153	14	120/0	No/Yes	9
h	12.3	40	131	-4	120/-40	No/No	24
i	11.1	51	145	51	-165/-40	No/No	26
j	13.6	30	173	29	162/13	No/Yes	5
k	14.4	25	-179	18	120/41	Yes/Yes	2
l	13.8	28	153	-12	77/-13	No/Yes	5
m	13.6	28	-178	25	77/61	No/Yes	4
n	14.5	25	167	3	47/20	Yes/Yes	0
o	14.7	23	-179	-6	-60/41	Yes/Yes	0

[a] T calculated using Eq. (1) from the main text.

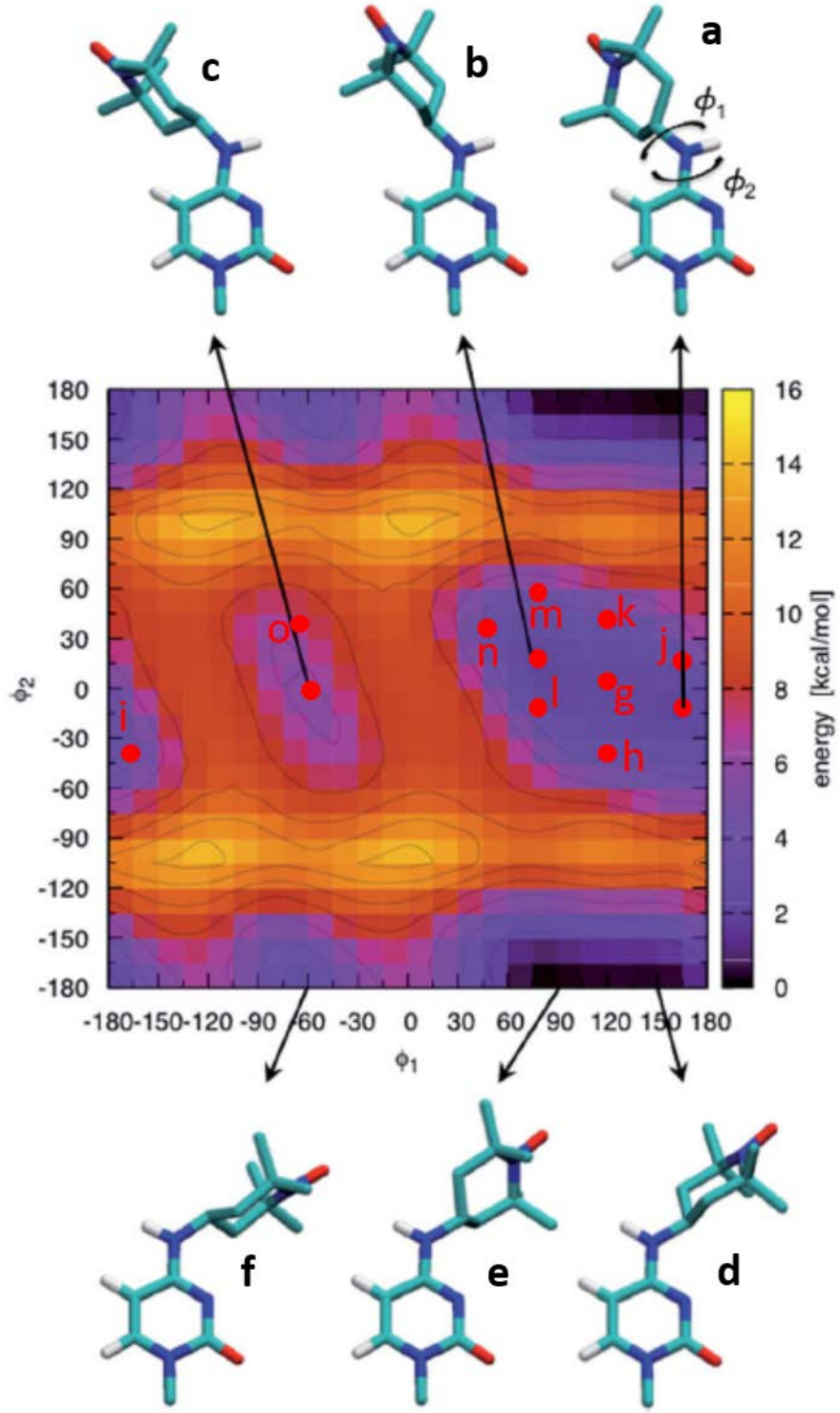

Figure S18. Potential energy surface of the C^T label as a function of the two indicated dihedral angles adapted from Halbmair *et al.*[23] The positions of the conformers on the potential energy surface **a** – **c** and **g** – **o** are marked by red.

5.1. Using individual conformers from the potential energy surface to simulate ENDOR spectra

To test whether or not the individual conformers are suited models to explain the ENDOR data of **RNA1** and **RNA2**, simulations based on the respective geometrical parameters *R*, α, and β of the individual conformers have been performed with anisotropic linewidth parameters as discussed in the main text. These simulations reveal that conformations in the vicinity of conformer **b** on the potential energy surface appear to be suited to simulate the ENDOR data for both RNAs using only a single conformation with the linewidth parameter specified in the main text (Table 2). Conformations located in the second minimum near conformation **c** also yield reasonable agreement between simulation and experiment. In contrast, conformations in the vicinity of conformation **a** yield bad agreement between spectral simulation and experiment. Additionally, it was noted that the number of short contacts with interatomic distances below 2.9 Å between non-hydrogen atoms of the C^T label and the A-RNA backbone is significantly higher for those conformations that produce ENDOR simulations which deviate strongly from the experimental spectra. Thus, the A-RNA conformation of the backbone appears to be predominant even after introducing the C^T label, in agreement with previous PELDOR results.[23] As ENDOR probes a smaller distance range than PELDOR, the present results indicate that the backbone structure is not strongly perturbed even in close vicinity of the C^T label.

RNA1 with its smaller inter-spin separation reacts more sensitive to the changes in distances induced by rotation about the dihedral angles. For **RNA1**, the geometrical parameters of conformer **n** clearly lead to the best agreement between simulation and experiment, as depicted in Figure S15, the spectra based on all other conformers are shown in Figure S19. Noteworthy, conformer **n** also shows a ^{19}F – nitroxide distance within the uncertainty given for the read-off analysis in the main text. The only other conformations which also yield acceptable simulations use conformer **b**, which is close to **n** on the potential energy surface and also only outside the uncertainty range of T_{sim} by 1 kHz (or 0.1 Å in the distance regime), and conformation **o**, again close to the best conformer (taking into account the separation by a high energy barrier) and within the uncertainty range. Conformations **m** and **k** deliver good simulations in some orientations and also in the non-selective spectrum, but the orientation selection at position A is already notably different from experimental observations. Consistently, these ‘almost acceptable’ conformers are also close to the best conformer **n**. All other conformers yield simulations that deviate more strongly from the data.

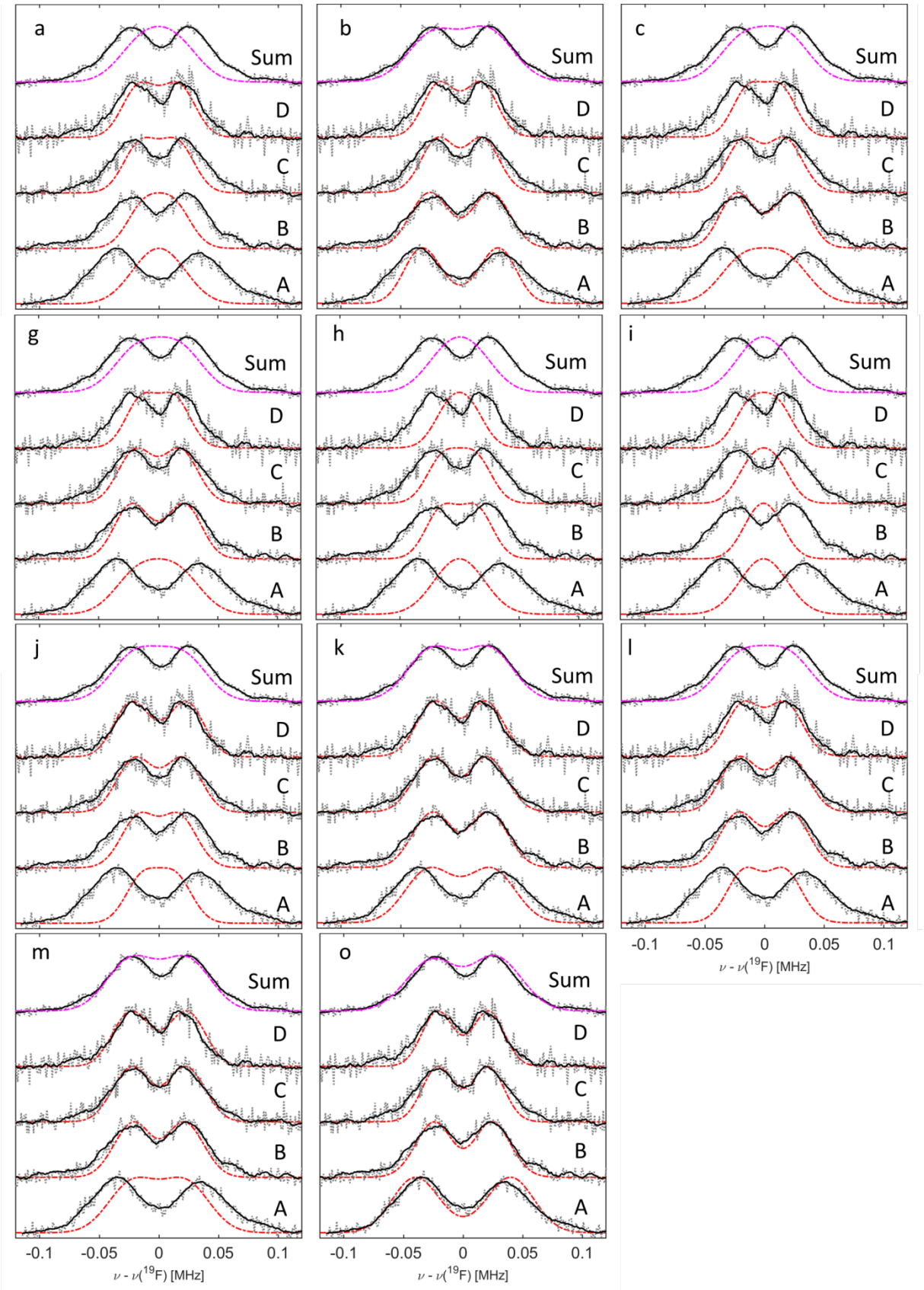

Figure S19. Simulations of the ENDOR spectra of **RNA1** using the conformers indicated in Figure S18, except **n**, which is already shown in Figure S15.

RNA2 reacts not as sensitive to the changes in distances induced by rotation about the dihedral angles ϕ_1 and ϕ_2 as **RNA1**, the results being summarized in Figure S20. Here, conformers **c** and **k** – **o** yield simulations of practically identical quality. Also **g** and **j** yield acceptable simulations, albeit the peak positions appear to be somewhat too far away from the Zeeman frequency of ^{19}F. Since **b** actually corresponds to the lowest point in the large basin of the potential energy surface shown in Figure S18 and is also more or less in the middle of all acceptable conformers, this conformer was considered to be best suited (the simulations are already shown in Figure S15). Conformers **a**, **h**, and **i** yield simulations which clearly do not fit. This is in agreement with the uncertainty range of the read-off analysis given in the main text, which covers all the conformers yielding acceptable simulations but exclude the conformers **a**, **h**, and **i**. These last conformers also lead to an abundance of close contacts with the RNA backbone. Finally, it is remarked that the behavior in **RNA2** mirrors the observations made on **RNA1**, in that the C^T spin label appears to clearly favor conformations centered around **b** and avoids conformations around **a**. Thus, the analysis of the RNA data provides a self-consistent picture which also agrees with the analyses provided earlier in the framework of a PELDOR study.[23]

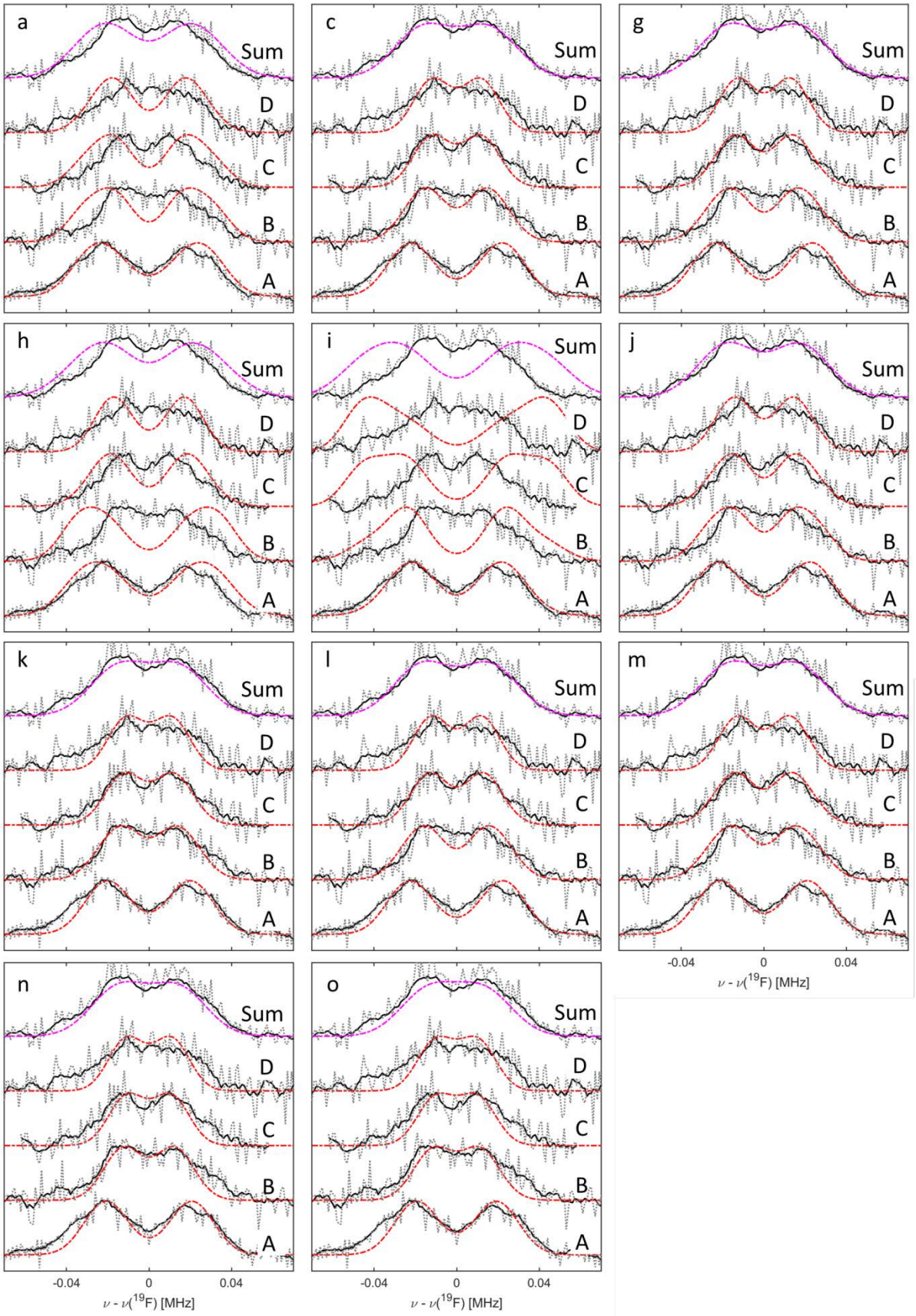

Figure S20. Simulations of the ENDOR spectra of **RNA2** using the conformers indicated in Figure S18, except **b**, which is already shown in Figure S15.

5.2. Using several conformers from the potential energy surface to simulate ENDOR spectra

ENDOR spectra contain information about the interspin separation and about the orientation of the dipolar vector within the molecular framework. Conversely, if this information is known for all molecules within the sample, it should be possible to obtain simulations that closely resemble the experimental data without using large, anisotropic linewidths, as these linewidth variations would then be implicit in the distribution of conformers. As several conformers have been modeled, this hypothesis was tested for **RNA1**. For that, the spectral simulations have been repeated including the isomers **b**, **n**, and **o** but with a considerably reduced and isotropic linewidth of only 20 kHz, close to the values used for model compounds **2** and **3**. It was found, that the linewidth in the orientation selective spectra is still too low, despite the presence of three different coupling constants and three different set of Euler angles (Figure S21a). It was furthermore found, that increasing the spread in coupling constants only slowly increased the width of the individual spectra. In contrast, decreasing the orientation selection by increasing the MW excitation bandwidth used in the simulations by a factor of 3 significantly improved the simulations of the orientation selective spectra (Figure S21b). Similar effects were obtained by using constant coupling constants but introducing a spread in the Euler angles α and β (the non-selective spectra are not affected by this). Noteworthy, when all 12 conformers were included in the simulations with increased excitation bandwidth, almost no orientation selectivity was observed in the simulated spectra. Thus, the right balance between distance and angular distribution has to be established without including too many conformers to reproduce the experimental data. These observations indicate that it is indeed possible to extract detailed information about conformational distributions from the ENDOR data, but also highlights that robust approaches to data analyses need to be developed.

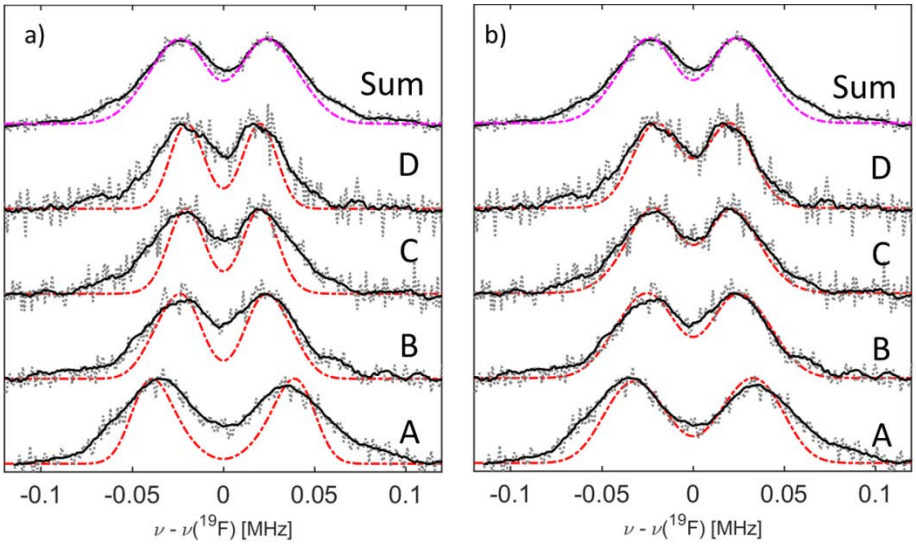

Figure S21. Simulations of the ENDOR spectra of **RNA1** including **b**, **n**, and **o** indicated in Figure S18 using an isotropic linewidth parameter of 20 kHz. The difference between a) and b) is that the excitation bandwidth is increased by a factor of 3 in b), to effectively introduce a larger variation in the orientations that contribute to the spectra.

6. The distributed dipole model

As discussed in the main text, the simplest approach for measuring distances between ^{19}F nuclei and an electron is to treat the electron as fully localized particle, residing in an “effective localization site”. For nitroxides, the midpoint of the N-O bond is already established as this effective site from PELDOR/DEER studies.[24] The next degree of precision is reached when the approximation of full localization is dropped and replaced by a distributed point dipole. In the case of the nitroxide, this could mean to treat the electron spin density as distributed between the nitrogen and the oxygen atom with spin populations of ρ_N and ρ_O, respectively. If the vectors from the ^{19}F atom to the two atoms of the nitroxide are parallel, the resulting equation for the coupling constant T would be (eq. (S8)):

$$T = 74.52 \cdot MHz \cdot \text{Å}^3 \cdot \left(\frac{\rho_N}{R_{N-F}^3} + \frac{\rho_O}{R_{O-F}^3}\right) \quad \text{(S8)}$$

In eq. (S8), R_{N-F} and R_{O-F} correspond to the distance between the F and the N or O atoms, respectively. Since $R_{N-F}^3 = (R_{midpoint} \pm \frac{d}{2})^3$ and $R_{O-F}^3 = (R_{midpoint} \mp \frac{d}{2})^3$, where *d* is the N–O bond length, notable deviations between the midpoint model and the distributed dipole model are expected for short distances.

7. References

[1] G. Sheldrick, *Acta Crystallogr. Sect. A* **2015**, *71*, 3–8.
[2] G. M. Sheldrick, *Acta Crystallogr. Sect. C Struct. Chem.* **2015**, *71*, 3–8.
[3] *X-RED, Data Reduction Program for Windows*, STOE & CIE, Darmstadt, Germany, Darmstadt, Germany, **2002**.
[4] L. Büttner, J. Seikowski, K. Wawrzyniak, A. Ochmann, C. Höbartner, *Bioorg. Med. Chem.* **2013**, *21*, 6171–6180.
[5] G. Sicoli, F. Wachowius, M. Bennati, C. Höbartner, *Angew. Chem. Int. Ed.* **2010**, *49*, 6443–6447.
[6] W. Bruggemann, J. R. Niklas, *J. Magn. Reson. A* **1994**, *108*, 25–29.
[7] B. Epel, D. Arieli, D. Baute, D. Goldfarb, *J. Magn. Reson.* **2003**, *164*, 78–83.
[8] S. Stoll, A. Schweiger, *J. Magn. Reson.* **2006**, *178*, 42–55.
[9] K. Möbius, A. Savitsky, *High-Field EPR Spectroscopy on Proteins and Their Model Systems: Characterization of Transient Paramagnetic States*, Royal Society Of Chemistry, **2008**.
[10] A. Schweiger, G. Jeschke, *Principles of Pulse Electron Paramagnetic Resonance*, Oxford University Press On Demand, **2001**.
[11] P.-P. Zänker, G. Jeschke, D. Goldfarb, *J. Chem. Phys.* **2005**, *122*, 024515.
[12] J. Tao, J. P. Perdew, V. N. Staroverov, G. E. Scuseria, *Phys. Rev. Lett.* **2003**, *91*, 146401.
[13] A. Schäfer, H. Horn, R. Ahlrichs, *J. Chem. Phys.* **1992**, *97*, 2571–2577.
[14] F. Neese, *Wiley Interdiscip. Rev. Comput. Mol. Sci.* **2012**, *2*, 73–78.
[15] M. D. Hanwell, D. E. Curtis, D. C. Lonie, T. Vandermeersch, E. Zurek, G. R. Hutchison, *J. Cheminformatics* **2012**, *4*, 17.
[16] F. Weigend, R. Ahlrichs, *Phys. Chem. Chem. Phys.* **2005**, *7*, 3297–3305.
[17] S. Grimme, J. Antony, S. Ehrlich, H. Krieg, *J. Chem. Phys.* **2010**, *132*, 154104.
[18] S. Grimme, S. Ehrlich, L. Goerigk, *J. Comput. Chem.* **2011**, *32*, 1456–1465.
[19] A. D. Becke, E. R. Johnson, *J. Chem. Phys.* **2005**, *123*, 154101.
[20] D. Margraf, D. Schuetz, T. F. Prisner, J. W. Bats, *Acta Crystallogr. Sect. E Struct. Rep. Online* **2009**, *65*, o1784–o1784.
[21] A. Meyer, G. Schnakenburg, O. Schiemann, *Acta Crystallogr. Sect. E Crystallogr. Commun.* **2015**, *71*, 1245–1249.
[22] A. Meyer, J. Wiecek, G. Schnakenburg, O. Schiemann, *Acta Crystallogr. Sect. E Crystallogr. Commun.* **2015**, *71*, 870–874.
[23] K. Halbmair, J. Seikowski, I. Tkach, C. Höbartner, D. Sezer, M. Bennati, *Chem. Sci.* **2016**, *7*, 3172–3180.
[24] C. Riplinger, J. P. Kao, G. M. Rosen, V. Kathirvelu, G. R. Eaton, S. S. Eaton, A. Kutateladze, F. Neese, *J. Am. Chem. Soc.* **2009**, *131*, 10092–10106.

APPENDIX A: Coordinates of compounds 1 – 4 in different conformations obtained by DFT

Conformer 1a

C	1.64524983711429	1.19214570865298	0.52153078042290
C	1.90535386419702	-0.04646349717693	-0.04088831872072
C	2.82005551920184	-0.90200284963153	0.56229634131670
C	3.46816768678215	-0.51862133221817	1.73060886999944
C	3.21090562968638	0.72373041188363	2.29908275872397
C	2.30498728570278	1.56671202987579	1.68388617672236
F	2.06772573695005	2.78325639249632	2.20477263053556
O	0.79863316056152	2.07506610238231	-0.13319372084598
H	4.18021037360081	-1.18355732899577	2.20356768256786
H	3.70290919963819	1.05302005165850	3.20514796511408
H	1.38792647725156	-0.32166469453617	-0.95115169031476
H	3.02347451406909	-1.86794453891560	0.11826428283766
C	-0.37878590101864	2.41423369483217	0.49711559516839
C	-1.12521798809218	3.40624046673980	-0.28575652063968
C	-0.70017501785098	4.00135069722138	-1.40482641259544
C	-2.50274466075977	3.86124923412460	0.12837470543405
O	-0.73244856282936	1.92862069315007	1.54148262357131
C	-1.69870426383755	4.96004216953024	-1.97015794610944
C	-2.51839113558345	4.62987596446736	1.45172996805226
C	-3.53982167021541	2.73759026435070	0.13894015124930
N	-2.79900770582946	4.79599208548697	-0.98999935631280
C	-2.18788467696915	4.56397150648692	-3.36775666623685
C	-1.21269291253036	6.41411144954384	-1.96444027098491
O	-3.88220559314081	5.44956783430592	-1.06812800308962
H	-0.83593894055624	6.69394046629740	-0.97971287061231
H	-2.05231637348442	7.06351075007781	-2.21809442528417
H	-0.41865957010638	6.55273371662620	-2.70134528729354
H	-2.50062796113848	3.51912315690600	-3.38733432262978
H	-1.39458892502521	4.71222920512103	-4.10366867688626

H	-3.03992740984474	5.19278678415379	-3.63114016189633
H	-2.31794622598352	3.94835180385508	2.27807447327393
H	-3.50199992122454	5.08413164143801	1.58023904131930
H	-1.76373519789561	5.41881309970012	1.44878634671893
H	-3.34344751732966	2.05980729568033	0.96934070220927
H	-3.50997295854473	2.17596758539481	-0.79711571417936
H	-4.53222443606160	3.17694688485788	0.25208646693412
H	0.25951624109654	3.82386509417627	-1.87080719753939

Conformer 1b

C	1.65089398716204	1.24932745020696	0.62310906768825
C	1.31627830861470	-0.06988819443847	0.89342470200812
C	2.27546337552926	-0.92257973521272	1.42901854839770
C	3.56303789325622	-0.46593469780731	1.68873641643133
C	3.90371855290034	0.85369491523706	1.41567924409020
C	2.94092917047780	1.69317569018756	0.88905249275170
F	3.25300196468898	2.97419355875278	0.61613566163672
O	0.80000926512735	2.15612022658033	0.01423948778742
H	4.30779820682573	-1.13456335182902	2.10204545863581
H	4.89634325875284	1.24309745646080	1.60237953236522
H	0.31372376514592	-0.41625013179703	0.68932703503220
H	2.01154572394609	-1.95079299305376	1.64076246600992
C	-0.47456584864349	2.33421556959429	0.49370616247589
C	-1.17506588021712	3.36820081171173	-0.27761283423298
C	-0.64361163070966	4.11756139212067	-1.24954943741015
C	-2.62352970251886	3.69729298237740	-0.01535081544643
O	-0.93742443197308	1.71688857821973	1.42105966810541
C	-1.62120240811905	5.08380209715758	-1.83852768897225
C	-2.86357909341110	4.31541680318692	1.36442809112809
C	-3.57189541314659	2.52304990180695	-0.25754508310600
N	-2.83579395974194	4.72782670289402	-1.06581889588948
C	-1.87274057333458	4.85216027661600	-3.33199977503247

C	-1.25069344203019	6.54918034957477	-1.57934185047774
O	-3.93934777181771	5.33287867326555	-1.21689622220305
H	-1.03997550535341	6.71612378432257	-0.52220824268276
H	-2.09138592671871	7.17921112440065	-1.87536436742185
H	-0.37238943574712	6.82838577702446	-2.16497630007152
H	-2.10350668873113	3.80429172681626	-3.52874473933763
H	-0.99392542534311	5.13836472778762	-3.91407912645819
H	-2.72023800267729	5.46471513147646	-3.64449993841224
H	-2.71959966890544	3.56069698617705	2.13765186491988
H	-3.88614895591458	4.69361475973328	1.40625253719683
H	-2.17426610864469	5.14298684615145	1.54116817672185
H	-3.44081756013673	1.77398171132022	0.52350992952050
H	-3.37828858284577	2.06479578741456	-1.22988156585626
H	-4.59880555189307	2.89153149698267	-0.24194823550635
H	0.38170409614712	4.05195580857995	-1.58753142438569

Conformer 1c

C	1.23542885537979	1.21132006280397	1.13228378150136
C	2.49730439451688	1.54169787421795	1.59712582517163
C	3.32979502631655	0.54834257117078	2.10121931255506
C	2.89849630001662	-0.77284553020178	2.13419705772333
C	1.63158758751563	-1.10889995907879	1.66957301388954
C	0.81333706950315	-0.11018652809880	1.17672068175002
F	-0.42410136474448	-0.41169744255240	0.74677784972839
O	0.37392520549692	2.21328315138622	0.70514805962537
H	3.54538838180755	-1.54865921516446	2.52416904736832
H	1.26591277478971	-2.12775497270001	1.68668057977985
H	2.81102902199404	2.57758944789337	1.55908749898407
H	4.31508948076764	0.80951563603321	2.46522560888333
C	0.04886678014346	2.23972469398435	-0.63391063850055
C	-0.90798368305206	3.32384138903454	-0.91324775605135
C	-1.27996138999614	3.61592071467574	-2.16332519919950

C	-1.57039061284113	4.21536553580111	0.11234847231250
O	0.51681893994506	1.47925990581431	-1.44001411063692
C	-2.24396018935999	4.75444765434415	-2.23919894076581
C	-0.60741617071935	5.12484105911702	0.87986850121654
C	-2.49719327863907	3.46813925426684	1.07386426051948
N	-2.39862643582390	5.05644717660992	-0.79620627074288
C	-3.60113964448682	4.36535636549154	-2.83489875254759
C	-1.67003689841503	5.97864448851469	-2.96359821717938
O	-3.13897966783995	5.99313707446791	-0.37132429107199
H	-0.68838840643718	6.23882275481683	-2.56521086707638
H	-2.34677282411896	6.82193113096476	-2.81463054095824
H	-1.57771941489267	5.77878792060641	-4.03328242480080
H	-3.99892793061431	3.47600106986310	-2.34431213800760
H	-3.50308704407553	4.16853338010205	-3.90445859504190
H	-4.29812808992062	5.19225012206713	-2.68646489430209
H	-0.05266076578674	4.55076051384870	1.62074659946203
H	-1.19227993603501	5.89708543475644	1.38239986534638
H	0.09783917977834	5.60579209439984	0.19897963617247
H	-1.91404592626645	2.87589882733350	1.77903271240914
H	-3.16957787584131	2.80652838626832	0.52437461716034
H	-3.09398689828464	4.19945743215360	1.62230807003129
H	-0.91980454977993	3.09005052498803	-3.03823741470741

Conformer 2a

C	1.626121486	1.180130962	0.548364942
C	2.203183566	0.246633464	-0.302504488
C	3.170553643	-0.616531905	0.195071399
C	3.558243119	-0.555602773	1.528273543
C	2.954190949	0.391098814	2.336328939
C	1.990133420	1.274387611	1.884484742
H	1.545631524	1.993012996	2.555465207
O	0.734633447	2.065697706	-0.042915496

H	4.307883944	-1.217536901	1.941186545
F	3.322747158	0.466095248	3.632574278
H	1.894231453	0.212893674	-1.338806428
H	3.628336861	-1.345301241	-0.462321547
C	-0.418162931	2.447645763	0.594588790
C	-1.156482122	3.416195401	-0.224725868
C	-0.750861128	3.915079950	-1.396896511
C	-2.496013759	3.958229577	0.207002509
O	-0.769642786	2.030941054	1.671229786
C	-1.726811062	4.879764110	-1.988061596
C	-2.429940058	4.801665365	1.481949407
C	-3.580193109	2.885525350	0.319239134
N	-2.789571413	4.839682588	-0.954989931
C	-2.292159777	4.409625354	-3.332900480
C	-1.168183185	6.302366011	-2.106026509
O	-3.842096391	5.541170096	-1.034311166
H	-0.740460691	6.630668029	-1.157674274
H	-1.981012941	6.977250600	-2.378735385
H	-0.395430176	6.343184070	-2.877099233
H	-2.656051545	3.383722932	-3.262166038
H	-1.522378347	4.461545757	-4.106082084
H	-3.122125437	5.060792491	-3.611731796
H	-2.236191866	4.159733760	2.341100050
H	-3.385361198	5.311647418	1.614558337
H	-1.639085930	5.551019983	1.408859101
H	-3.384781020	2.249933660	1.182560150
H	-3.606708579	2.268104143	-0.581002370
H	-4.548133666	3.375288030	0.437046432
H	0.180008547	3.662220854	-1.885852090

Conformer 2b

C	1.690065505	1.294877127	0.631253011

C	1.340842848	-0.047165653	0.684740614
C	2.267000886	-0.954954006	1.184199800
C	3.520412671	-0.539971720	1.621256151
C	3.819782464	0.808022223	1.546550720
C	2.929104133	1.746663345	1.058795506
H	3.191405489	2.794707864	1.008665003
O	0.855987461	2.254439180	0.066892289
H	4.252886101	-1.234816612	2.009687429
F	5.030649961	1.234374335	1.964029733
H	0.366925941	-0.371259167	0.349867415
H	2.008923958	-2.005663765	1.232411132
C	-0.443638450	2.359329028	0.494210715
C	-1.155351325	3.392953719	-0.266621476
C	-0.648014501	4.117383667	-1.269161559
C	-2.594245253	3.732697516	0.027766556
O	-0.918112663	1.690360492	1.379044761
C	-1.636339075	5.075378216	-1.852034196
C	-2.796580451	4.341345486	1.417301884
C	-3.557665646	2.567340232	-0.201358456
N	-2.818618016	4.773083462	-1.010048389
C	-1.956880149	4.782386949	-3.321953968
C	-1.231903151	6.542986164	-1.672894230
O	-3.926305647	5.372701554	-1.151223312
H	-0.972365904	6.750544401	-0.633760945
H	-2.074073872	7.175528999	-1.958656986
H	-0.375660471	6.781001990	-2.307420679
H	-2.214434568	3.731279447	-3.459611046
H	-1.098548112	5.023448670	-3.952902280
H	-2.805816347	5.396879264	-3.626085735
H	-2.638034527	3.579185614	2.180523920
H	-3.815402834	4.724732977	1.489675231
H	-2.098158530	5.163700803	1.582696580

H	-3.418153422	1.813994869	0.573731598
H	-3.385767525	2.110674941	-1.178516011
H	-4.580360521	2.945857157	-0.165906946
H	0.364503542	4.033951231	-1.640063830

Conformer 2c

C	1.27538678901515	1.28640987346017	1.16895331188225
C	2.12748831044344	1.78232853010091	2.14715473516007
C	2.98259404281011	0.90956534407286	2.80649575227011
C	2.99268374689692	-0.44518820739292	2.49553837189996
C	2.12317830954047	-0.89043251711912	1.51608916044430
C	1.25138237741269	-0.06037964490047	0.83431647998565
H	0.59716110181952	-0.45579323184021	0.07341791021105
O	0.39344711344458	2.20929098378667	0.61996376309710
H	3.65015229133156	-1.14535117142966	2.99315490354407
F	2.11579693938892	-2.20389628202746	1.20501901205176
H	2.10721111542497	2.83795400895551	2.38305451037239
H	3.64836787675845	1.28833116878899	3.57227190577539
C	0.05291716999254	2.17878316756676	-0.70814807095164
C	-0.91690085926026	3.24719624647793	-1.00148288666196
C	-1.40899717345752	3.42115964044762	-2.23204282729854
C	-1.47420253337785	4.24002576515609	-0.00748909920721
O	0.49571336250687	1.39183852051601	-1.50628799857714
C	-2.37957365069357	4.55236346659895	-2.32139156733346
C	-0.43213227880110	5.17669401907126	0.60692906294355
C	-2.34339406319125	3.60413168763332	1.08071038477304
N	-2.34506337329417	5.03265602516602	-0.91915670205243
C	-3.79992380754043	4.09775106790858	-2.67745459007332
C	-1.91907302214025	5.67148085075177	-3.26094296774342
O	-3.06166110274799	5.99431663217207	-0.50991455244000
H	-0.89531197898157	5.97105036484953	-3.03277637007402
H	-2.57700402566184	6.53252183851525	-3.13090608581219

H	-1.96871299698875	5.33904673753087	-4.29998785158792
H	-4.11891497786410	3.27995573060242	-2.02923155292319
H	-3.84137814237018	3.76439458216823	-3.71615754884565
H	-4.48072729437670	4.94008560174684	-2.54437830829912
H	0.16872523008185	4.64351807515994	1.34251087309076
H	-0.95399370720634	6.00057057477536	1.09619496908658
H	0.22464222998508	5.58429506207127	-0.16373174851606
H	-1.72156709744525	3.06606683439732	1.79585671366500
H	-3.06453085409520	2.91001599830207	0.64402922083751
H	-2.88735537524321	4.39653582024565	1.59754482946531
H	-1.13836969211570	2.80868683571354	-3.08264514215849

Conformer 2d

C	1.12279901100049	1.05323196063425	1.05236730813211
C	2.39635833654710	0.89923795005274	0.52078265835022
C	3.25294269763032	-0.02325222473553	1.10953723986425
C	2.85907116463690	-0.77725020450926	2.20862046866564
C	1.58257666852463	-0.58302691624758	2.70364478252235
C	0.69439892837007	0.31959087115891	2.14918403482752
H	-0.29689952217913	0.45224923495790	2.56007520149191
O	0.22224156349286	2.00784718223185	0.59115134416073
H	3.51567528577353	-1.49802676741149	2.67748040580017
F	1.18030759997926	-1.30008044711944	3.77404963261050
H	2.70548798755820	1.47633651482033	-0.33663866872129
H	4.24797240558628	-0.15587756896847	0.70368376016438
C	0.04855078150044	2.21969614433430	-0.75237951220159
C	-0.88879715932334	3.33332881478408	-0.97506989143280
C	-1.16521566193594	3.76211378882741	-2.21023776961200
C	-1.61961253371037	4.12024477805985	0.08958699251098
O	0.59223850512870	1.57828915397876	-1.61567674607961
C	-2.11512916673577	4.91294273165815	-2.23440355326154
C	-0.70681321527051	4.92111708710624	1.02185156518569

C	-2.62867338974715	3.29750434599759	0.89439481937477
N	-2.36579150666684	5.07017609927550	-0.78224754784472
C	-3.42833795372224	4.59791540958141	-2.95763384020168
C	-1.48248749679260	6.19386755681815	-2.79136289486573
O	-3.13905230556617	5.95926813201524	-0.31578451253583
H	-0.53506624530666	6.40408035872987	-2.29261468227203
H	-2.16505548781927	7.02740523305060	-2.61819390097161
H	-1.30395537485954	6.09319901704540	-3.86377330682557
H	-3.86511141106219	3.67265751831585	-2.57883071473987
H	-3.25438287553536	4.49510704444236	-4.03091791052167
H	-4.12993805719535	5.41612893693995	-2.78602601438264
H	-0.20936321257494	4.25864798493269	1.72941407257177
H	-1.31897976147177	5.64064730603104	1.56871790262475
H	0.04842822649338	5.46454617532721	0.45115859579153
H	-2.11012430957216	2.63740074344831	1.58950526441961
H	-3.25614140281283	2.69764069587901	0.23236175194214
H	-3.26582138579018	3.98307315623400	1.45632012998534
H	-0.74023972657189	3.33000220232275	-3.10701646452610

Conformer 3a

C	1.707706013	1.349017539	0.697189412
C	1.665069873	1.022643592	2.045265963
C	2.586464356	0.113332223	2.547525983
C	3.522197870	-0.434438305	1.687885875
C	3.577564337	-0.111025260	0.344356687
C	2.651172915	0.795299658	-0.154432305
H	2.656872766	1.079755514	-1.198869016
O	0.866012559	2.309792516	0.141765453
F	4.417668368	-1.317478170	2.181085113
H	4.329056386	-0.561291672	-0.290873819
H	0.921247863	1.463737963	2.692303936
H	2.584353107	-0.170293611	3.591789125

C	-0.483509416	2.239658768	0.361622721
C	-1.172311625	3.347574190	-0.310323387
C	-0.586155549	4.308556529	-1.031327126
C	-2.669891687	3.503300837	-0.239826281
O	-1.019740478	1.377415920	1.015166412
C	-1.561384011	5.293915613	-1.588448888
C	-3.187149725	3.761692971	1.176999150
C	-3.430560874	2.349325548	-0.896091664
N	-2.827970585	4.733746732	-1.059365321
C	-1.593595491	5.297865249	-3.120505181
C	-1.354159987	6.713250167	-1.049518111
O	-3.955833218	5.265348294	-1.287543728
H	-1.300229346	6.708962977	0.040286657
H	-2.196096877	7.334499827	-1.359577276
H	-0.431523041	7.139094317	-1.449562384
H	-1.712461300	4.284722057	-3.507676338
H	-0.669596718	5.722944494	-3.518899373
H	-2.436325721	5.905229388	-3.454401674
H	-3.090402089	2.856597310	1.775976734
H	-4.237097009	4.053006830	1.120239418
H	-2.623293059	4.567313839	1.651144474
H	-3.328099160	1.448471368	-0.291182858
H	-3.042988567	2.153581874	-1.897549682
H	-4.484365243	2.621152384	-0.973584807
H	0.478454368	4.385040532	-1.208363896

Conformer 3c

C	1.137339640	1.087529875	1.086427227
C	1.407033688	-0.089007950	0.402613618
C	2.280329542	-1.009302748	0.966892615
C	2.850165900	-0.725011614	2.195204481
C	2.580560694	0.440601909	2.889096198

C	1.709798623	1.359983420	2.319259972
H	1.470102394	2.286339106	2.825328704
O	0.217908580	2.023661921	0.616047443
F	3.701478682	-1.622211626	2.738118209
H	3.044206490	0.619372630	3.849921134
H	0.952312258	-0.280871444	-0.557609076
H	2.520262547	-1.936959629	0.464342647
C	0.297774693	2.467108412	-0.677192167
C	-0.755343955	3.462296366	-0.937643790
C	-0.849215008	4.081232901	-2.118262719
C	-1.816897505	3.912434209	0.040512422
O	1.123420492	2.091825808	-1.471753874
C	-1.972331992	5.062827085	-2.178098148
C	-1.269808916	4.659832964	1.260100832
C	-2.782904652	2.806118030	0.470823133
N	-2.548216635	4.879049326	-0.824711296
C	-3.021819798	4.715605394	-3.238133785
C	-1.491501357	6.509106157	-2.344285664
O	-3.542082373	5.547286440	-0.410047953
H	-0.723711353	6.747682677	-1.606741770
H	-2.339741886	7.180459451	-2.201766397
H	-1.080876029	6.658912893	-3.344725321
H	-3.343097281	3.678012470	-3.138244605
H	-2.612274230	4.865575985	-4.239317946
H	-3.886591094	5.367836033	-3.106022022
H	-0.801174638	3.960842347	1.951879815
H	-2.101358101	5.160334219	1.758952239
H	-0.536559064	5.410134943	0.958838441
H	-2.288548245	2.117211179	1.155549451
H	-3.143848929	2.250495080	-0.396363297
H	-3.635572402	3.265135818	0.973536107
H	-0.180118775	3.899839965	-2.949844857

Conformer 4a

C	1.78798943220631	1.48639051698542	0.60055305109588
C	1.68357357518270	1.16466078461679	1.94684157058780
C	2.70299629784532	0.43650424520900	2.54006659106935
C	3.82438643261548	0.02463610387914	1.81434425925704
C	3.89432894304538	0.35727481878583	0.45899784346976
C	2.88299192679155	1.08443600237161	-0.14960327756156
H	2.93510868710834	1.34873745498972	-1.19829705063985
O	0.87498832541513	2.31702841840125	-0.04088722719064
C	4.91383255367404	-0.71905762690462	2.46912435199682
H	4.74075466988315	0.02484204980890	-0.13010048601942
H	0.82957104406562	1.48755748252151	2.52358092874849
H	2.64186698273379	0.21197114325240	3.59817761302846
C	-0.46737846177983	2.19448075163195	0.19292478582233
C	-1.20099777144307	3.31152793652951	-0.41449525828767
C	-0.67006309130371	4.29754398421434	-1.14479578377721
C	-2.69060739014492	3.45568391390661	-0.23629769863577
O	-0.97029442453361	1.28869587473269	0.81355005339806
C	-1.68885177686258	5.28512819883667	-1.61467469416163
C	-3.10618095316004	3.63748371924810	1.22567569839536
C	-3.49252242436549	2.33362066342659	-0.89885727744587
N	-2.90558008004524	4.73090954394325	-0.97124384217239
C	-1.86414623309984	5.28084594107127	-3.13729520165419
C	-1.42824840297219	6.70750580379715	-1.10665265479643
O	-4.05799790480661	5.22392638904589	-1.16115457549465
H	-1.23930710487654	6.70829168200031	-0.03195994060700
H	-2.30692566575645	7.32067162790515	-1.31293775448146
H	-0.56620771380796	7.13972316510067	-1.61866270889825
H	-2.04868582250098	4.26980769133046	-3.50299215474505
H	-0.97048189806087	5.67776729935122	-3.62384825641900
H	-2.71755872122277	5.90959282940590	-3.39546703115820

H	-2.98831256831682	2.69689113417301	1.76284654453190
H	-4.15118926404556	3.95042391274255	1.25913253071114
H	-2.49429932183066	4.40347660220456	1.70572271789127
H	-3.34340083514213	1.40355394065828	-0.35103376967990
H	-3.17535233404085	2.19241268381339	-1.93389127156893
H	-4.54980556318751	2.60236992171025	-0.88817529193408
H	0.38033077155763	4.39090558201722	-1.38698867688189
C	4.64362703860927	-1.68200130795969	3.44636857262315
C	5.67013841523352	-2.36608764436119	4.08207464822110
C	6.24720990433898	-0.46057374529781	2.13658478248113
C	7.28764906831397	-1.13155118288000	2.76267740405570
C	6.97491259726467	-2.07271345427141	3.72773794623582
H	6.47407265180340	0.30077598200954	1.39966119564262
H	3.61550237986549	-1.91549500776069	3.69722540695481
H	5.47317218614031	-3.11977547382697	4.83360502836913
H	8.32290254165341	-0.92546990177937	2.52244305590075
F	7.97917930195877	-2.72794045058634	4.34963530372318

Conformer 4c

C	1.60771503851965	1.60966034769935	1.00114294694114
C	1.77551484794328	0.33548149058078	0.47588495955163
C	2.72494573880490	-0.49908397196133	1.04503380105211
C	3.50449709233697	-0.09062228930474	2.13070695206308
C	3.29554765831692	1.19031596292706	2.64886280667830
C	2.35313013887565	2.03959061266265	2.08967051508547
H	2.19598088149650	3.03643397637497	2.48166048365882
O	0.63849381485830	2.49831998432712	0.54132429252660
C	4.52598924257703	-0.98694881776603	2.69900110660215
H	3.89899213904339	1.53735944436732	3.47933726926819
H	1.18124757937231	0.00365427469574	-0.36135295578912
H	2.84817493923945	-1.50013385761458	0.64984627959218
C	0.35641176896132	2.60404222774892	-0.79456464709486

C	-0.75974647498063	3.54041337064570	-1.00862949395765
C	-1.33429701541179	3.67114283623976	-2.20814808735833
C	-1.39708350435805	4.42497157632274	0.03803999453249
O	0.94094372489024	2.00598478477549	-1.66323321351174
C	-2.46048479671543	4.65157859167764	-2.21457412241257
C	-0.44188104433998	5.43791815072094	0.66911028187858
C	-2.16915752603407	3.65404343995422	1.11179775294059
N	-2.36983099342733	5.15548708969857	-0.82263874265777
C	-3.82899631485137	3.99263998904725	-2.43428315207092
C	-2.25951563281877	5.80504464172112	-3.19871486859279
O	-3.18471488608280	6.00716392303736	-0.35644984524210
H	-1.26863403380983	6.24731809738573	-3.08378056181218
H	-3.01238204273806	6.57021908320310	-3.00285427607834
H	-2.37356244952853	5.44626682337599	-4.22398387127095
H	-3.96528835954792	3.14762041901638	-1.75860322405515
H	-3.92230346214175	3.64175988897466	-3.46378013112435
H	-4.60622966099218	4.73248339370751	-2.23582433362860
H	0.24409537645129	4.93456715788866	1.35034378993154
H	-1.02851814941240	6.17095972999331	1.22518837436240
H	0.13414555544275	5.95785262394981	-0.09876369091904
H	-1.47902058844933	3.14577150680567	1.78430716156936
H	-2.82725964587156	2.91329621182830	0.65329971698013
H	-2.77702296426923	4.36148245682411	1.67892855943249
H	-1.02681164169384	3.12023668060941	-3.08746376357050
C	5.28072131907448	-1.81797086500467	1.86463853346258
C	6.24905954397193	-2.66710469598193	2.37970439306100
C	4.76912506595003	-1.02770630955279	4.07552506377203
C	5.73267979407222	-1.87196268753562	4.61003251985257
C	6.45531088254757	-2.67718110286391	3.74758215455001
H	4.17703858662937	-0.41023150333701	4.74064337043927

H	5.12577550296728	-1.77853052420580	0.79295286962635
H	6.84550264528184	-3.30506456223535	1.74026219457818
H	5.92183111384345	-1.91907468159071	5.67513085599304
F	7.39656119600684	-3.50207491983288	4.25692398116461

Appendix B: HPLC of Model Compounds 1 – 4

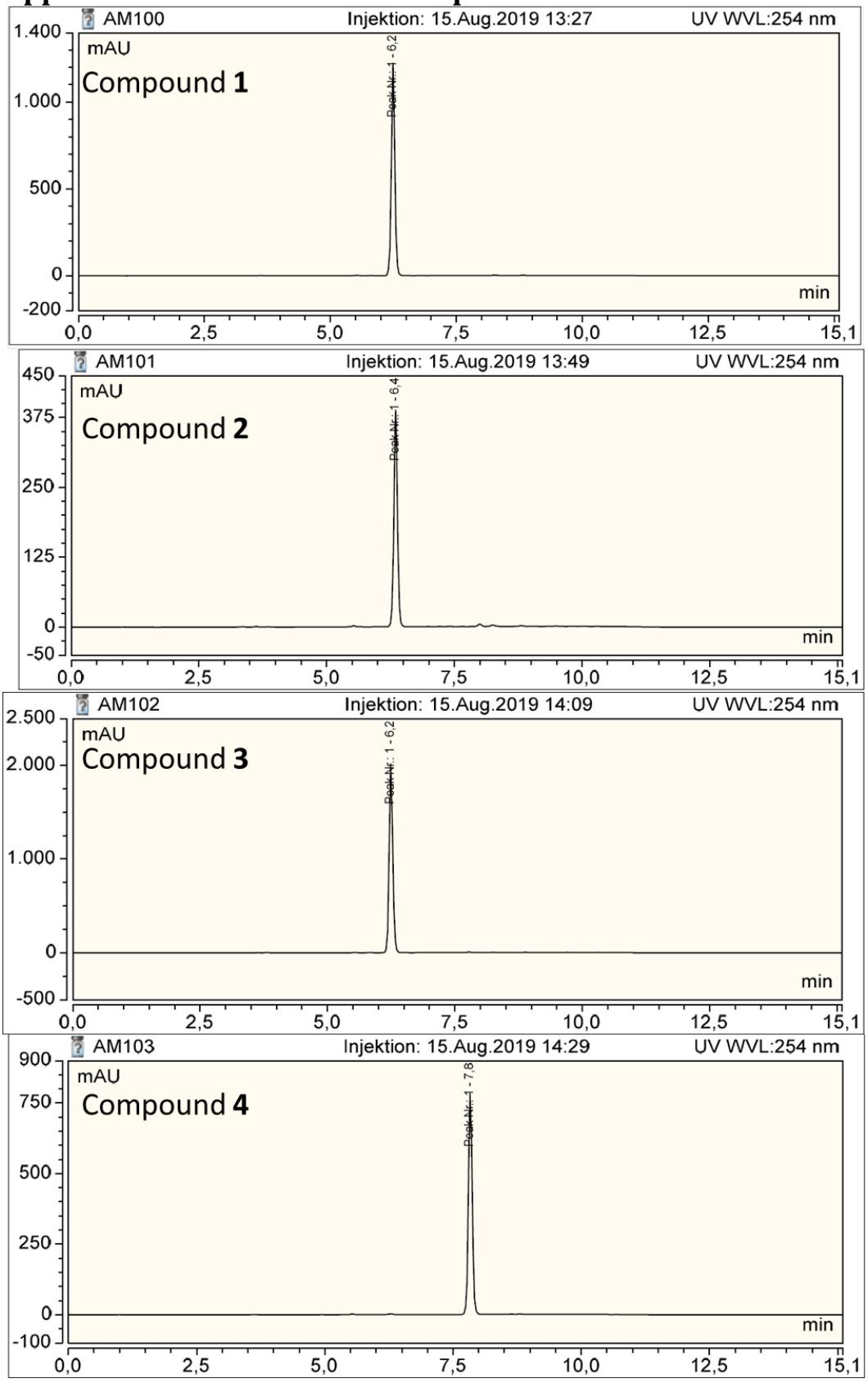

Figure S22. Chromatograms of **1** – **4**.

Appendix C: Analytics of the RNA systems

NMR Spectra of S4

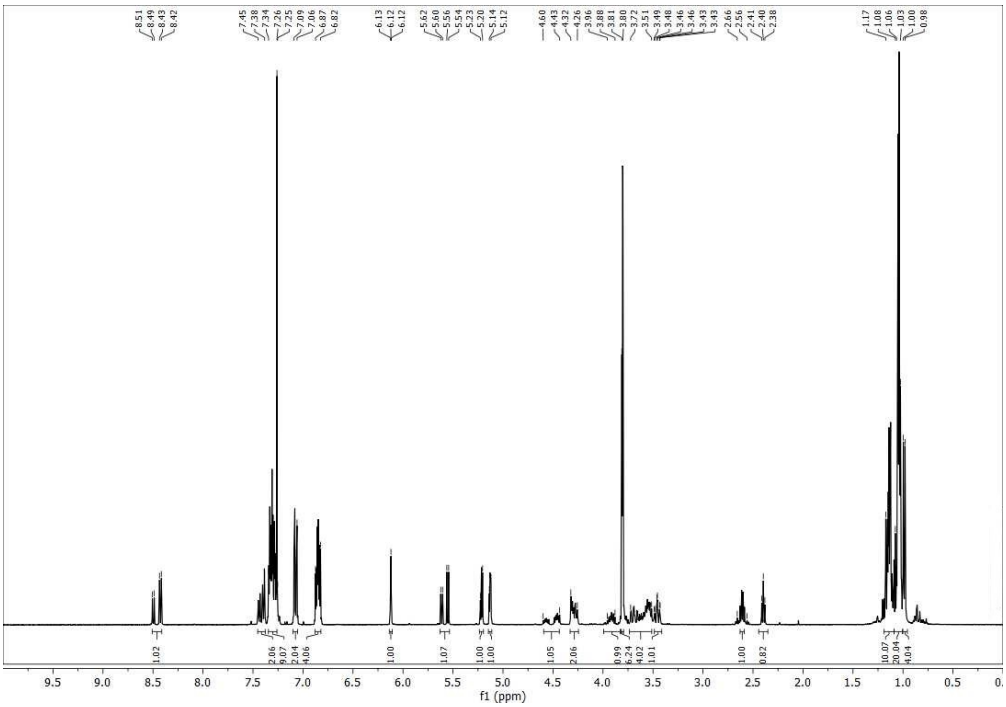

Figure S23. Compound S**4** ^{1}H NMR.

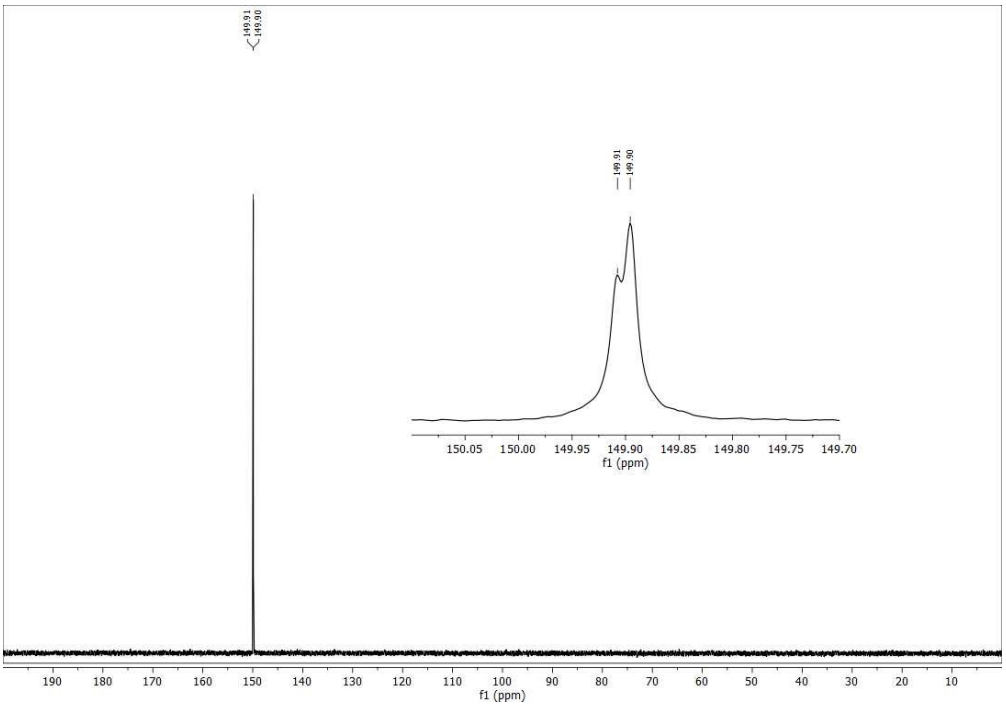

Figure S24. Compound S**4** ^{31}P NMR.

Anion exchange HPLC chromatograms of the RNAs

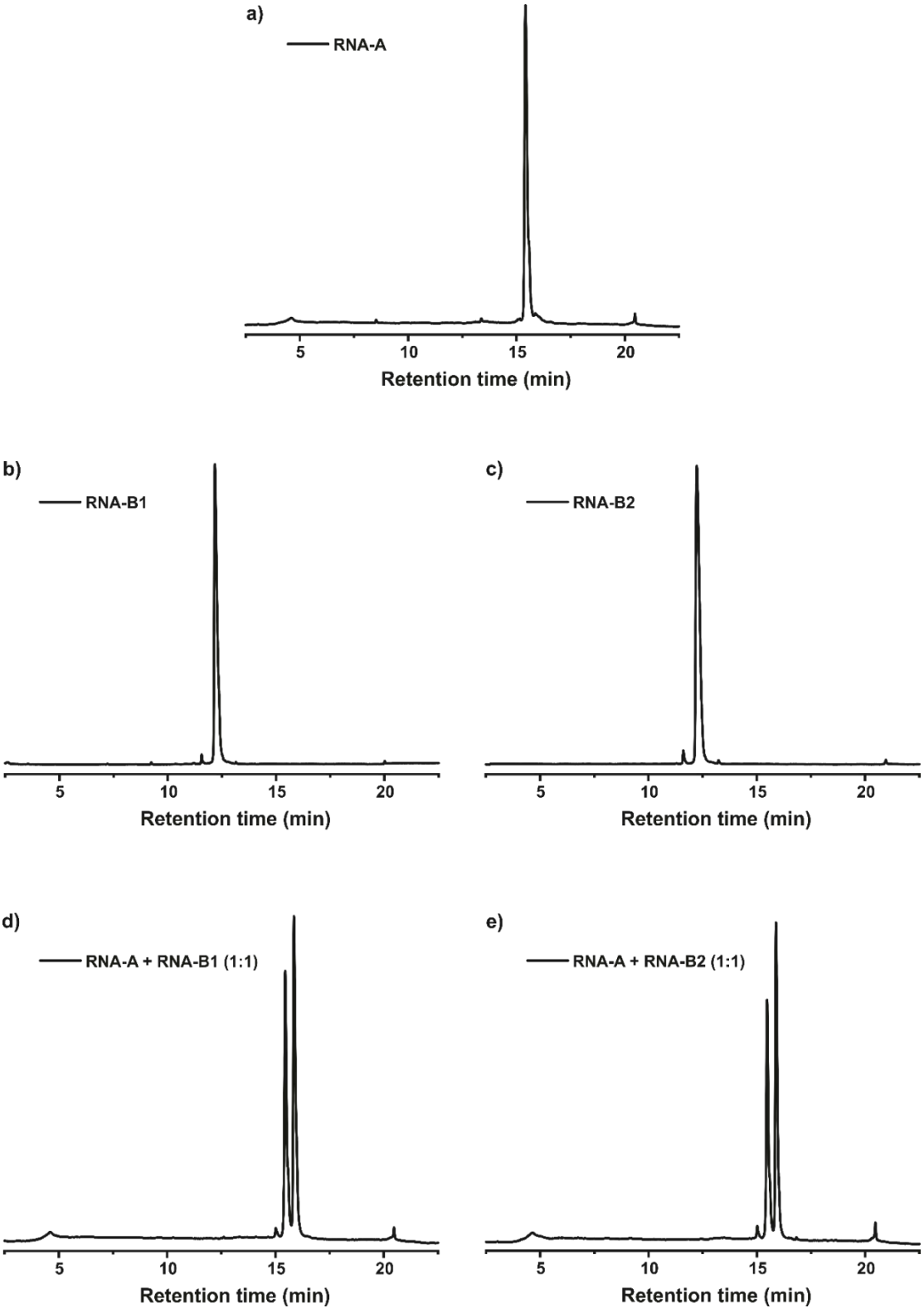

Figure S25. Anion exchange HPLC chromatograms of different RNA samples. a) RNA-A after purification. b) RNA-B1 after purification. c) RNA-B2 after purification. d) Equimolar mixture of RNA-A and RNA-B1. e) Equimolar mixture of RNA-A and RNA-B2.

HRMS analysis result of RNA-A

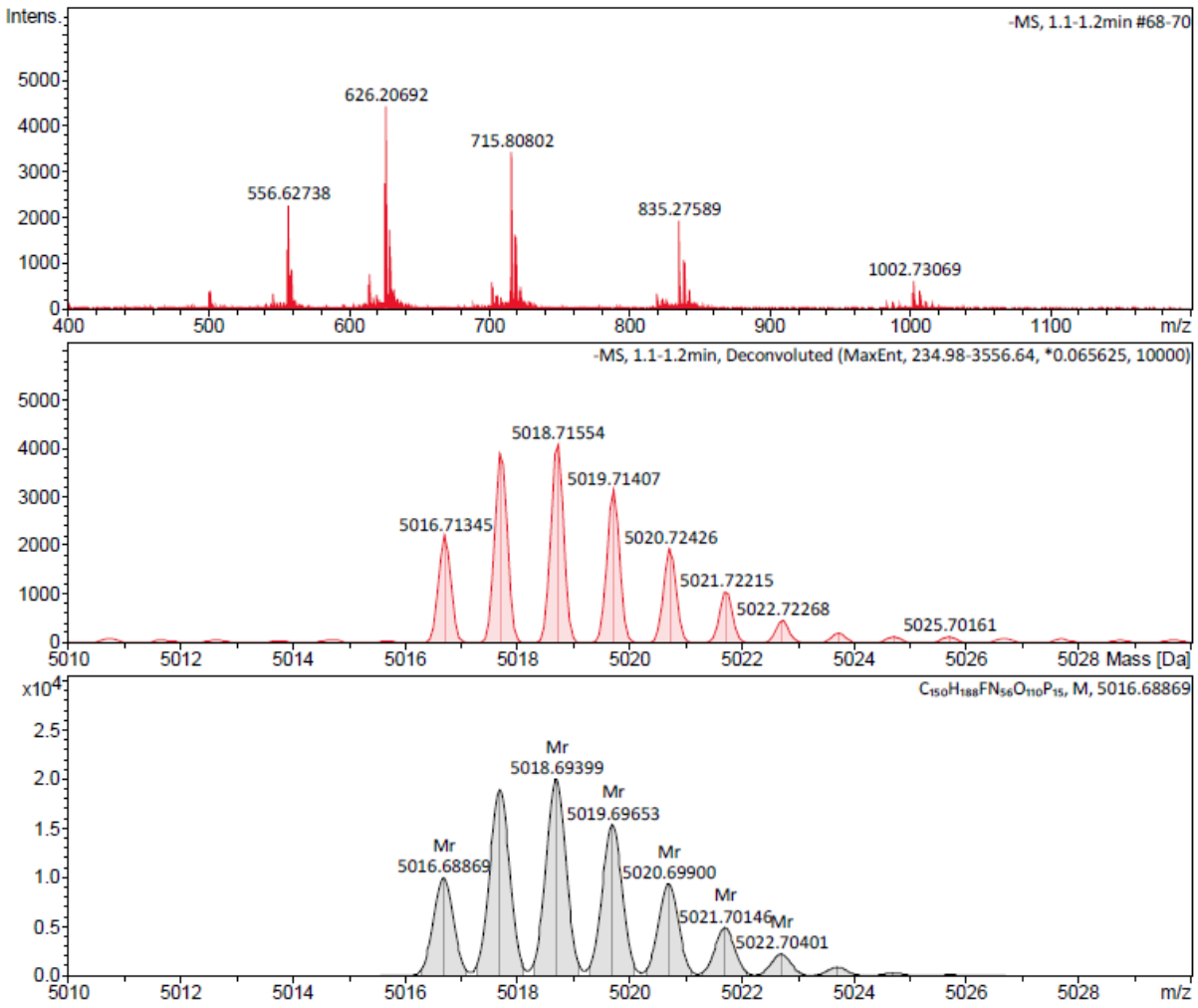

Figure S26. High resolution ESI mass spectrum of **RNA-A** along with simulation of the mass peaks (bottom).

HRMS analysis result of RNA-B1

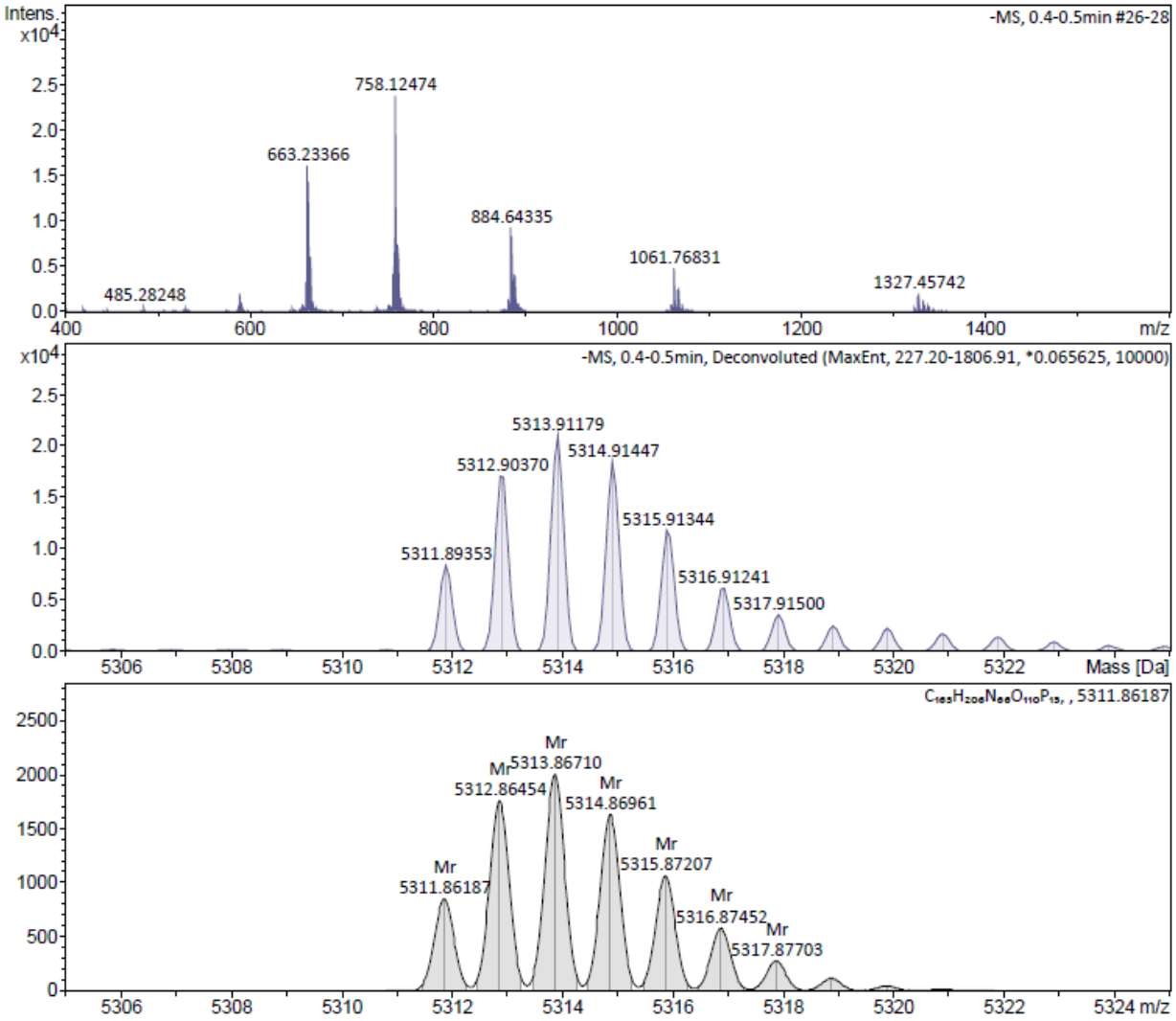

Figure S27. High resolution ESI mass spectrum of **RNA-B1** along with simulation of the mass peaks (bottom).

HRMS analysis result of RNA-B2

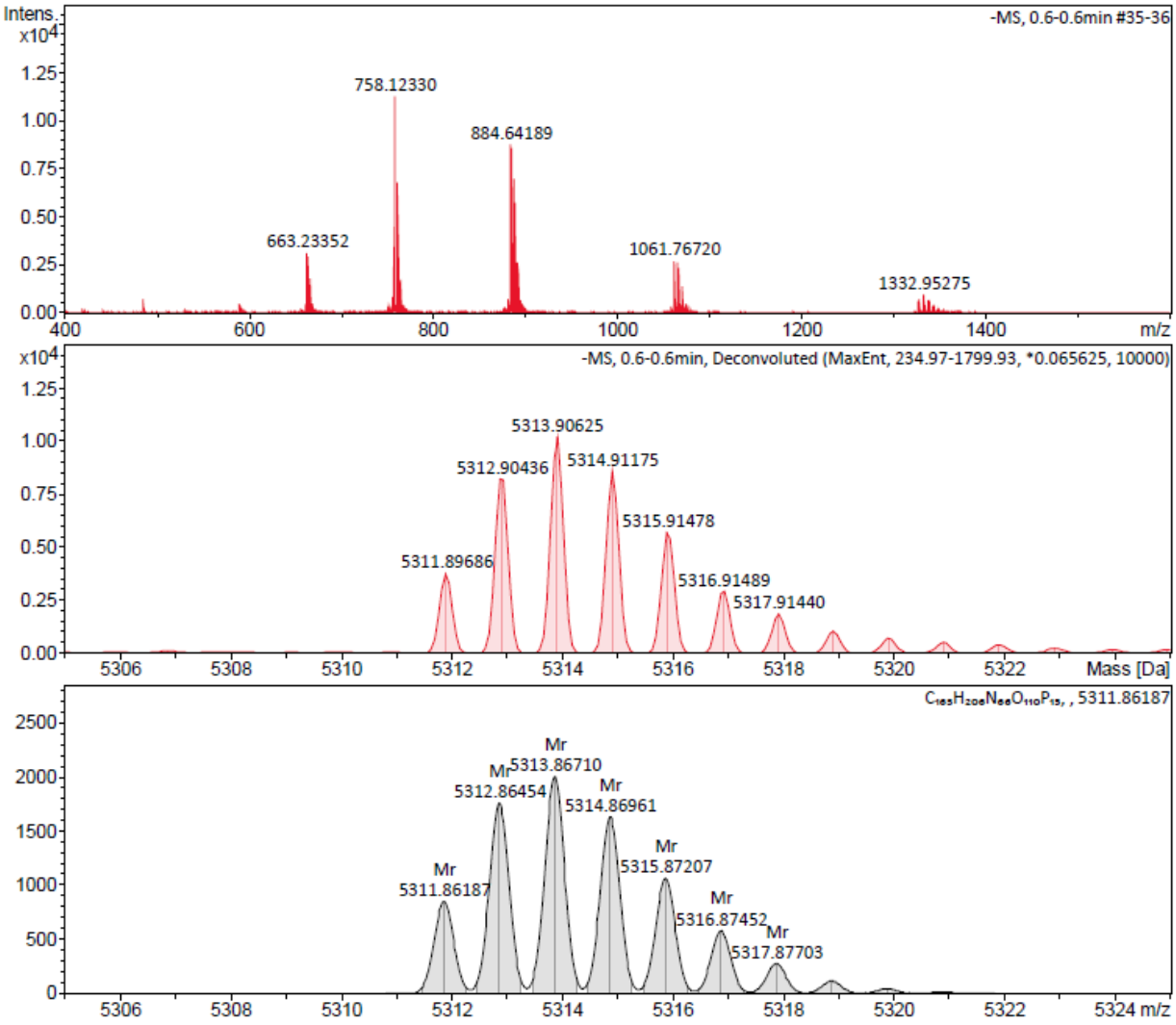

Figure S28. High resolution ESI mass spectrum of **RNA-B2** along with simulation of the mass peaks (bottom).